

**ISTANBUL TECHNICAL UNIVERSITY ★ GRADUATE SCHOOL OF SCIENCE**  
**ENGINEERING AND TECHNOLOGY**

**ACOUSTIC ANALYSIS OF AN UNDERWATER GLIDER**



**M.Sc. THESIS**

**Turgay HIZARCI**

**Department of Shipbuilding and Ocean Engineering**

**Shipbuilding and Ocean Engineering Programme**

**JUNE 2019**



**ISTANBUL TECHNICAL UNIVERSITY ★ GRADUATE SCHOOL OF SCIENCE**  
**ENGINEERING AND TECHNOLOGY**

**ACOUSTIC ANALYSIS OF AN UNDERWATER GLIDER**



**M.Sc. THESIS**

**Turgay HIZARCI**  
**(508161108)**

**Department of Shipbuilding and Ocean Engineering**

**Shipbuilding and Ocean Engineering Programme**

**Thesis Advisor: Assist. Prof. Dr. Bilge TUTAK**

**JUNE 2019**



**İSTANBUL TEKNİK ÜNİVERSİTESİ ★ FEN BİLİMLERİ ENSTİTÜSÜ**

**BİR SUALTI PLANÖRÜNÜN AKUSTİK ANALİZİ**

**YÜKSEK LİSANS TEZİ**

**Turgay HIZARCI  
508161108**

**Gemi ve Deniz Teknolojisi Mühendisliği Anabilim Dalı**

**Gemi ve Deniz Teknolojisi Mühendisliği Programı**

**Tez Danışmanı: Dr. Öğr. Üyesi Bilge TUTAK**

**HAZİRAN 2019**



Turgay HIZARCI, a M.Sc. student of ITU Graduate School of Science Engineering and Technology student ID 508161108, successfully defended the thesis entitled “ACOUSTIC ANALYSIS OF AN UNDERWATER GLIDER”, which he prepared after fulfilling the requirements specified in the associated legislations, before the jury whose signatures are below.

**Thesis Advisor :**      **Assist. Prof. Dr. Bilge TUTAK** .....  
Istanbul Technical University

**Jury Members :**      **Prof. Dr. Şakir BAL** .....  
Istanbul Technical University

**Prof. Dr. Cem GAZIOĞLU** .....  
Istanbul University

**Date of Submission : 03 May 2019**  
**Date of Defense : 12 June 2019**





*To my family and friends,*



## **FOREWORD**

I would like to thank all of the people who helped and pulled me up throughout the process of research, examination and correction of this thesis. However I can only name a few of them because of the limitations. First, I would like to thank people who make this research comes to an end. My thesis supervisor Assist. Prof. Dr. Bilge TUTAK share his time with me to finish this research instead of sharing that time with his family and I would like to thank him for making easier this process for me. I would like to thank my thesis committee members, Prof. Dr. Şakir BAL and Prof. Dr. Cem GAZİOĞLU, for all their guidance, ideas and feedbacks. I would also like to thank Mehmet Ozan ŞERİFOĞLU who is my business partner and one of my closest friend have helped a lot with sharing his knowledge, time and effort without hesitation. Gürbüz BİLİCİ helped me from the start, prepare the foundation of this research and I would like to show my gratitude to him. I am wishing the best for him and his family.

I would like to thank my parents and my brother for their assistance and for supporting me in any circumstances. They are the best.

I also would like to thank Yeşim ULUÇAY who bear with me throughout this period. This is the another chapter of our journey and cannot be done without her attention, support and kindness. Her support gave me the power to get through the real hard part of the process.

I hope this research influence people on underwater acoustic and help their study.

May 2019

Turgay HIZARCI  
Ocean Engineer



## TABLE OF CONTENTS

	<u>Page</u>
<b>FOREWORD</b> .....	<b>ix</b>
<b>TABLE OF CONTENTS</b> .....	<b>xi</b>
<b>ABBREVIATIONS</b> .....	<b>xiii</b>
<b>SYMBOLS</b> .....	<b>xv</b>
<b>LIST OF TABLES</b> .....	<b>xvii</b>
<b>LIST OF FIGURES</b> .....	<b>xix</b>
<b>SUMMARY</b> .....	<b>xxi</b>
<b>ÖZET</b> .....	<b>xxiii</b>
<b>1. INTRODUCTION</b> .....	<b>1</b>
1.1 Buoyancy Driven Underwater Gliders .....	3
1.2 Acoustics .....	8
1.2.1 Underwater acoustics .....	12
1.2.2 Environmental effects and regulations of underwater noise .....	14
<b>2. METHODS</b> .....	<b>17</b>
2.1 Mesh .....	17
2.2 CFD .....	18
2.3 Aeroacoustic Methods .....	20
<b>3. VALIDATION</b> .....	<b>25</b>
3.1 Mesh .....	25
3.2 Resistance .....	29
3.3 CFD Parameters and Flow Noise .....	30
<b>4. UNDERWATER GLIDER MODELLING</b> .....	<b>35</b>
4.1 Model, Mesh and CFD .....	35
4.2 Virtual Hydrophones .....	40
<b>5. RESULTS AND DISCUSSION</b> .....	<b>45</b>
<b>6. CONCLUSION</b> .....	<b>55</b>
<b>REFERENCES</b> .....	<b>59</b>
<b>CURRICULUM VITAE</b> .....	<b>63</b>



## **ABBREVIATIONS**

<b>ADCP</b>	: Acoustic Doppler Current Profiler
<b>ARGOS</b>	: Advanced Research and Global Observation Satellite
<b>ASV</b>	: Autonomous Surface Vehicle
<b>AUG</b>	: Autonomous Underwater Glider
<b>AUV</b>	: Autonomous Underwater Vehicle
<b>BEM</b>	: Boundary Element Method
<b>CAA</b>	: Computational Aero Acoustics
<b>CFD</b>	: Computational Fluid Dynamics
<b>CTD</b>	: Conductivity, Temperature, Depth
<b>DO</b>	: Dissolved Oxygen
<b>DB</b>	: Desibel
<b>FFT</b>	: Fast Fourier Transform
<b>FW-H</b>	: Ffowcs Williams-Hawkings
<b>GPS</b>	: Global Positioning System
<b>IMU</b>	: Inertial Measurement Unit
<b>OASPL</b>	: Over All Sound Pressure Level
<b>PAR</b>	: Photosynthetically Active Radiation
<b>RANS</b>	: Reynolds Averaged Navier Stokes
<b>RF</b>	: Radio Frequency
<b>ROV</b>	: Remotely Operated Vehicle
<b>SEL</b>	: Sound Exposure Level
<b>SONAR</b>	: Sound Navigation and Ranging
<b>SPL</b>	: Sound Pressure Level
<b>TBL</b>	: Turbulent Boundary Layer
<b>TKE</b>	: Turbulent Kinetic Energy
<b>UMS</b>	: Unmanned Maritime Systems
<b>USV</b>	: Unmanned Surface Vehicle
<b>UUV</b>	: Unmanned Underwater Vehicle



## SYMBOLS

$\rho$	: Density
$\nu$	: Kinematic Viscosity
$\delta(\mathbf{f})$	: Dirac Delta Function
$c$	: Speed of Sound
$C_f$	: Friction Coefficient
$D$	: Diameter
$H(\mathbf{f})$	: Heaviside Function
$I$	: Intensity
$k$	: Turbulence Kinetic Energy
$L$	: Vehicle Length
$P$	: Pressure
$T_{ij}$	: Lighthill's Stress Tensor
$t$	: Time
$\mathbf{u}$	: Velocity
$y^+$	: Dimensionless Wall Distance



## LIST OF TABLES

	<u>Page</u>
<b>Table 1.1</b> : Comparison of the UUV specifications.....	<b>2</b>
<b>Table 1.2</b> : Traveled distance for different frequencies and wavelengths .....	<b>9</b>
<b>Table 1.3</b> : Anthropogenic sound sources and possible effects .....	<b>15</b>
<b>Table 3.1</b> : Comparison of the CFD results with the experiment .....	<b>29</b>
<b>Table 3.2</b> : Virtual hydrophones locations. ....	<b>30</b>
<b>Table 4.1</b> : Virtual hydrophones coordinates for 0° attack angle case.....	<b>40</b>
<b>Table 5.1</b> : Total surface and quadrupole values of the Rudder Zone hydrophones. ....	<b>54</b>





## LIST OF FIGURES

	<u>Page</u>
<b>Figure 1.1</b> : Commercially used USV examples. ....	2
<b>Figure 1.2</b> : UUV examples.....	3
<b>Figure 1.3</b> : Sawtooth motion of an underwater glider. ....	4
<b>Figure 1.4</b> : Data transmitting and communication position of underwater glider. ...	5
<b>Figure 1.5</b> : Modular sensor payload section of an underwater glider. ....	8
<b>Figure 1.6</b> : Directivity pattern of monopole source.....	11
<b>Figure 1.7</b> : Directivity pattern of dipole source. ....	12
<b>Figure 1.8</b> : Directivity pattern of quadrupole source.....	12
<b>Figure 1.9</b> : Ambient noise spectra for different activities. ....	14
<b>Figure 2.1</b> : Comparison of the some turbulence models. ....	19
<b>Figure 3.1</b> : Dimensions of the computational domain.....	26
<b>Figure 3.2</b> : Mesh domain. ....	27
<b>Figure 3.3</b> : Mesh inside of the domain. ....	27
<b>Figure 3.4</b> : Mesh of the domain and the refinement boxes.....	28
<b>Figure 3.5</b> : Mesh around the body.....	28
<b>Figure 3.6</b> : Boundary layer.....	28
<b>Figure 3.7</b> : Top view of DARPA Suboff model.....	29
<b>Figure 3.8</b> : Calculated DARPA Suboff sound pressure levels to the 10 kHz.....	31
<b>Figure 3.9</b> : Comparison of the methods to the 1000 Hz. ....	32
<b>Figure 3.10</b> : Flow noise spectra comparison in Point X11. ....	32
<b>Figure 4.1</b> : Side view of the underwater glider. ....	35
<b>Figure 4.2</b> : Top view of the underwater glider.....	35
<b>Figure 4.3</b> : Computational domain dimensions of the underwater glider.....	36
<b>Figure 4.4</b> : Domain of the underwater glider case and location.....	37
<b>Figure 4.5</b> : Mesh inside of the domain for underwater glider case. ....	37
<b>Figure 4.6</b> : Mesh of the refinement zones and surface from top.....	37
<b>Figure 4.7</b> : Mesh of the refinement zones and surface from side.....	38
<b>Figure 4.8</b> : Mesh of the refinement zones from side for +10° angle of attack.....	38
<b>Figure 4.9</b> : Mesh of the refinement zones from side for -10° angle of attack. ....	38
<b>Figure 4.10</b> : Boundary layer of underwater glider case for 0° angle of attack. ....	39
<b>Figure 4.11</b> : Visualization of the first group virtual hydrophones for 0° angle of attack. ....	42
<b>Figure 5.1</b> : OASPL values in XY plane for 0° angle of attack case (both directions show positive values). ....	45
<b>Figure 5.2</b> : OASPL values in XY plane for -10° angle of attack case (both directions show positive values). ....	46
<b>Figure 5.3</b> : OASPL values in XY plane for 10° angle of attack case (both directions show positive values). ....	46
<b>Figure 5.4</b> : Flow parameters (velocity, turbulent kinetic energy and pressure) and magnitudes of the 0° angle of attack case. ....	47
<b>Figure 5.5</b> : Flow parameters (velocity, turbulent kinetic energy and pressure) and magnitudes of the -10° angle of attack case. ....	48

<b>Figure 5.6 :</b> Flow parameters (velocity, turbulent kinetic energy and pressure) and magnitudes of the 10° angle of attack case. ....	<b>48</b>
<b>Figure 5.7 :</b> Surface pressure distributions (0°, -10°, 10° respectively) and magnitudes of all cases. ....	<b>49</b>
<b>Figure 5.8 :</b> OASPL values in XZ plane (top view) for 0° angle of attack case. ....	<b>50</b>
<b>Figure 5.9 :</b> OASPL values in XZ plane (top view) for -10° angle of attack case....	<b>50</b>
<b>Figure 5.10 :</b> OASPL values in XZ plane (top view) for 10° angle of attack case. ...	<b>51</b>
<b>Figure 5.11 :</b> Total Surface and Quadrupole terms of Rudder Zone at 10° angle of attack. ....	<b>52</b>
<b>Figure 5.12 :</b> Vorticity field for 3 different angle of attack cases. ....	<b>53</b>
<b>Figure 5.13 :</b> Vorticity flow field at the back of the underwater glider in XY plane for 10° angle of attack.....	<b>54</b>



# ACOUSTIC ANALYSIS OF AN UNDERWATER GLIDER

## SUMMARY

Buoyancy driven underwater gliders are the unmanned and autonomous vehicles that use buoyancy engine to change vehicle's buoyancy to create a vertical motion by pumping the hydraulic oil to the external bladder from an internal reservoir. This vertical motion transferred to horizontal movement with the flow passing through the wings and hull of the vehicle. This motion mechanism create the most important feature of the vehicle which is high endurance. Endurance of the underwater gliders can reach up to 12 months and can collect data from the ocean with the sensors throughout the expedition. Collected data can be sent to control center periodically with the satellite connection.

In this thesis, acoustic analysis of an underwater glider is made using STAR-CCM+ CFD software. Validation of the case, models and parameters are done with the DARPA Suboff model and results from the literature. K-epsilon turbulence model form URANS turbulence model family is used for modelling the turbulence with  $y^+$  value selected and set around 50 for both validation and glider cases. Ffowcs Williams-Hawkings analogy is used for the calculation of the flow noise.

Glider cases are carried out in 3 different angles of attack as  $0^\circ$  - $10^\circ$  and  $10^\circ$  in 1 m/s flow speed. Selected angle of attacks are generally the maximum angles for the gliders for ascending and descending. Gliders travel with the angle of attack to create a lift force for horizontal movement, to increase the range. Therefore,  $-10^\circ$  and  $10^\circ$  angle of attack cases simulate the real life situations of the vehicle. Sound Pressure Level in decibels is compared with the all three angle of attack cases. Monopole, dipole and quadrupole sound terms are analyzed.

The results showed that, although the glider is very quiet in  $0^\circ$  angle of attack, increasing angle of attack affects the flow noise production of the vehicle substantially by creating more complex flow topology around the glider. Moreover, physical parameters such as velocity, vorticity, turbulent kinetic energy and pressure change cause variations in the Over All Sound Pressure Level of the regions which means hydrodynamic parameters and design of the vehicles are crucial for acoustic performance. These OASPL values are measured in simulation with virtual hydrophones. Virtual hydrophones are placed according to the flow field and wake zone and elongate to the positive x direction from the back of the glider. Virtual hydrophones are located in  $0^\circ$  angle of attack case and rotated as required to logical comparison for  $-10^\circ$  and  $10^\circ$  angle of attack cases. Due to their generic capabilities, gliders are becoming an important part of many naval forces. However, the results suggest that the acoustic properties of these vehicles should be more carefully inspected for military applications. On the other hand, due to newer EU regulations underwater noise is also getting more interest because of its effect on the marine mammals. Therefore, the generated underwater noise from gliders should be more thoroughly considered.



## BİR SUALTI PLANÖRÜNÜN AKUSTİK ANALİZİ

### ÖZET

Su altı ve su üstü verisi toplama sistemleri teknolojinin ilerlemesi ile birlikte insana bağlı olmaktan kurtulup insansız ve otonom sistemlere yönelmektedir. Bu şekilde zorlu çevre şartları ve ulaşması zor derinliklerin üstesinden gelinebilmektedir. Bu tarz araçlar hem askeri, endüstriyel ve bilimsel amaçlar için özelleştirilebilmekte ve kullanılmaktadır. Bu araçlar en geniş kategoride İnsansız Deniz Araçları olarak bilinmektedir. Daha sonrasında su altı ve su üstü araçları olarak ayrılarak İnsansız Su Üstü Araçları ve İnsansız Su Altı Araçları olarak bölünebilmektedir. Su altı araçları ise kullanım alanlarına ve şekillerine bağlı olarak şekillenerek Uzaktan Kumandalı Su Altı Araçları, Otonom Su Altı Araçları ve Otonom Su Altı Planörleri olarak 3 gruba ayrılabilir.

Otonom Su Altı Planörleri kendilerine özel hareket mekanizması ve bu hareket mekanizmasının getirdiği özellikler sayesinde diğerlerinden ayrılmaktadır. Bu araçların en büyük özelliği hacim değişime dayalı hareket sistemleridir. Diğer deniz araçlarında kullanılan aksine bu araçlarda pervane bulunmamaktadır. Su altı planörleri esas olarak su kolonunda dalış ve çıkış hareketi gerçekleştirir. Çıkış hareketini başlatabilmek için araç içinde bir rezervuarda yer alan hidrolik yağ, pompa yardımıyla aracın dışında yer alan kauçuk bir balona benzeyen yapıya pompalanır. Hacmini değiştirebilen bu yapıya basılan hidrolik yağ aracın toplam ağırlığını değiştirmeden toplam hacmin artmasını sağlar. Bu sayede araç artan kaldırmanın kuvvetinin verdiği ekstra kuvvetle yüzeye doğru hareket eder. Dalış hareketi için ise bu işlemlerin tersi gerçekleştirilir ancak bu işlem pompa kullanılmadan pasif olarak gerçekleştirilmektedir. Böylece enerji tasarrufu sağlanmaktadır. Araç bahsedilen dalış ve çıkış hareketlerini arka arkaya tekrarlayarak hareket eder. Bu kendini tekrarlayan hareket düzeni testereye benzediğinden dolayı testere dişi adı verilmiştir.

Pervane gibi sürekli bir motorun kullanılması gereken sevk sistemi yerine bu tarz bir sevk sistemi seçilmesinin sebebi pillerin kullanımının azaltılarak aracın dışarıdan müdahaleye ihtiyaç duymadan çalışabilme süresini uzatmaktır. Su altı planörleri 6 ay ile 12 arası bir süre boyunca çalışabilmektedir. Bu sayede geniş alanları tarayabilmekte ve 10.000 km gibi büyük mesafeler kat edebilmektedir.

Su altı planörlerinin ortalama faydalı yük kapasiteleri 5 kg civarındadır. Bu faydalı yük kapasitesi sensörler için kullanılmaktadır. Görevin ihtiyaçlarına göre CTD, ADCP, PAR, DO, nitrat sensörü gibi sensörler araca yerleştirilebilmektedir. Böylece su altı planörleri su kolonundan istenilen verileri sürekli olarak toplayabilmektedir. Toplanan veriler periyodik olarak su yüzeyinde uydu bağlantısı kurularak kontrol merkezine iletilmekte ve kullanıcıların hizmetine sunulmaktadır. Su altında iletişim kurabilmek için öncelikle ses dalgaları ile iletişim kurulabilen cihazlar yerleştirilmesi gerektiği için genel olarak su altında iletişimin olmadığını varsayabiliriz. Bu nedenle bu işlemler araçta bulunan antenlerin su yüzünden dışarıya çıkartılmasıyla gerçekleştirilmektedir.

Su altı planörleri sürekli kontrol merkeziyle iletişim halinde olamadığı için otonom olarak hareket etmektedir. Navigasyon araç içinde yer alan IMU, pusula, basınç ölçer ve altimetre gibi sensörler kullanılarak gerçekleştirilmektedir. Araç su yüzeyindeyken aldığı görev konumuna, GPS'den alınan ilk konum verisi ve navigasyon sensörlerinden gelen verileri birleştirerek ulaşabilmektedir. Pervane gibi bir itki sistemi olmadığından dolayı mevki hassasiyeti pervane kullanan araçlara göre düşüktür ancak istenilen standartları karşılayabilmektedir.

Su altı planörleri akustik olarak sürekli hareket eden ve titreşim yayan bir motor kullanılmadığı için oldukça verimli araçlardır. Ancak su altı araçlarında ses kaynağı olarak sadece araç içinde yer alan teçhizatlar gösterilmemektedir. Su altındaki akıntıların ve aracın oluşturduğu hareketin sonucu olarak araç etrafından geçen akım da bir ses oluşturmaktadır. Bu şekilde oluşan seslere akım sesi veya hidrodinamik ses denilebilmektedir ve dikkate alınması gereken bir veridir. Bu tarz araçlarda oluşan toplam ses seviyesine oldukça katkı sağlamaktadır.

Bu tezde bir su altı planörünün CFD analizi STAR-CCM+, CFD yazılımı kullanılarak yapılmış ve akustik analizi Ffowcs Williams-Hawkins analojisi Farassat 1A formülü eklenerek yapılmıştır. Türbülans modellemesi URANS türbülans modeli ailesinden k- $\omega$  türbülans modeli kullanılarak gerçekleştirilmiştir.  $y^+$  değeri doğrulama ve diğer tüm su altı planörü senaryolarında 50 civarında tutulmuştur.

Doğrulama, DARPA Suboff modelinin akustik sonuçlarının literatürde bulunan araştırmalarla karşılaştırılması sonucunda oluşturulmuştur. İlk olarak seçilen CFD parametrelerinin doğruluğu, atılan ağ örgüsünün uyumluluğu ve ağ örgüsü sıklaştırma bölgelerinin doğruluğu aracın deney sonuçlarıyla karşılaştırılarak değerlendirilmiştir. Akustik sonuçlar için ise toplam SPL değerleri ve 0 - 1000 Hertz aralığındaki SPL değerleri karşılaştırılmıştır.

Su altı planörü simülasyonları ise  $0^\circ$ ,  $-10^\circ$  ve  $10^\circ$  atak açılarında gerçekleştirilmiştir. Bunun sebebi su altı planörlerinin gerçek dünya koşullarında ileri hareket oluşturabilmesi için atak açısı ile ilerlemeleri gerekmektedir. Bu sayede kanatlardan geçen akım ile kaldırma kuvveti oluşturulabilmektedir. Bu şekilde simülasyonlarda gerçek koşullar ele alınmıştır.

Sonuçlarda, diğer su altı araçlarıyla kıyaslandığında yavaş sayılabilecek bir araç olan su altı planörlerinin dikkate alınması gereken seviyede hidrodinamik ses çıkardığı görülmüştür. Bu sese etki eden önemli parametrelerden biri takıntılardır. Takıntılarının uçlarında oluşan uç girdapları akışı bozarak ses seviyesini arttırmaktadır.

Analizlerde atak açısı ile gerçekleşen hareketin ses üretimine etkisinin oldukça büyük olduğu görülmüştür. Bunun sebebi atak açısı arttığında hız vektörleri, türbülans kinetik enerjisi, girdaplık ve basınç gibi fiziksel parametreleri değişmesidir. Aracın arkasından x doğrultusunda ilerleyen şekilde yerleştirilen sanal hidrofondan ölçülen verilerde  $0^\circ$  atak açısında maksimum değerin 70 dB iken,  $-10^\circ$  atak açısında bu değerin 102 dB,  $10^\circ$  atak açısında ise 120 dB'e çıktığı görülmüştür.

Ses; monopol, dipol ve quadropol olmak üzere 3 terime ayrılabilir. FW-H analojisinde ise sırasıyla loading, thickness ve kuadropole adını almaktadır. Monopol ve dipol terimler yüzeyden oluşmaktadır. Kuadropol terim ise hacimde oluşmaktadır. Su altı için yapılan akustik analizlerde en önemli katkının monopol terimlerden geldiği görülmektedir. Ancak monopol terimler araçtan uzaklaştıkça hızlıca azalmaktadır ve analizlerin sonuçlarında girdaplığın arttığı bölgelerde kuadropol terimlerin de önem kazandığı görülmektedir.

Fiziksel parametreler aracın dizaynı ve hidrodinamik özellikleriyle birebir ilişkili olduđu için aracın optimizasyonun yapılması ve sensör yerlerinin buna göre belirlenmesi gerekmektedir. Sesin özellikle askeri açıdan önemli olduğunu düşündüğümüzde bu araçların ses seviyesinin azaltılması ve oluşan seslerin anlaşılabilmesi oldukça önemlidir.





## 1. INTRODUCTION

Oceans create crucial resources for continued human life. Over %50 percent of the World's oxygen is produced by the oceans and absorb substantial amount of carbon dioxide. Currents that flow around the oceans regulate the climate. Marine transportation is most important part of the international trades. Apart from providing sea food, oceans provide crucial ingredients of many medical products (US Department of Commerce, n.d.-b). Owing to these data oceans create and sustain life. Considering the importance of the oceans, knowledge about the oceans is limited and mostly lies in shallow waters (US Department of Commerce, n.d.-a).

Currently, increasing the knowledge about the deep oceans depends on Unmanned Maritime Systems (UMS). Because they can withstand the pressure of deep waters, can be programmed for abundant amount of missions with different sensor payload, are able to operate with minimum requirement to people and can operate in harsh environment. These properties create interest, increase and expand the usage of the UMS's by scientists and commercial applications. In addition, due to the importance of marine environment it is generally very important for military applications, too. Marine environment can be characterized in 2 major parts as pelagic (water column) and benthic (sediment bottom) (Michael John Kingsford, n.d.). UMS mostly focus on pelagic zone because most of the marine life exists, most of the military activity and all marine transportation occur in pelagic zone.

Categorization of the UMS's starts with the separation of the sea surface. There are 2 main vehicle group in UMS as Unmanned Surface Vehicles (USV) and Unmanned Underwater Vehicles (UUV).

USV can be customized for military and commercial use. Variety of the usage areas of the USV can be exemplified as Mine Counter Measure (MCM), Intelligence, Surveillance and Reconnaissance (ISR), Anti Submarine Warfare (ASW), Fast Inshore Attack Craft (FIAC), oil and gas discovery, oceanographic data collection,

hydrographic, oceanographic and environmental explorations. Some examples of the USV can be seen in Figure 1.1.



**Figure 1.1 :** Commercially used USV examples (L3 ASV, 2016).

UUV are subcategorized after their specialized abilities for the users need. There are 3 main UUV types as Autonomous Underwater Vehicles (AUV), Remotely Operated Vehicles (ROV) and Autonomous Underwater Gliders (AUG). All these underwater vehicles have their own unique abilities, different endurance, different usage areas, different advantages and disadvantages. Despite AUV and ROV use of propellers to move themselves, AUG use buoyancy and center of gravity change mechanism to increase the endurance. Comparison of the some of significant UUV specifications are presented seen in the Table 1.1.

**Table 1.1 :** Comparison of the UUV specifications.

Characteristics	AUV	ROV	AUG
Endurance	1-2 week	10-15 hours	6-12 months
Autonomy	Medium	Low	High
Speed	5 m/s	2 m/s	0.3 - 1.5 m/s
Propulsion	Propellers	Propellers	Buoyancy Mechanism
Location Accuracy	High	High	Low

As can be seen in Table 1.1 different type of UUV's provide distinct capability for users. Commercially used UUV's examples can be seen in Figure 1.2. (From left to right, AUV – ROV – AUG)



**Figure 1.2 :** UUV examples (Unmanned Systems Technology, n.d.) (Diver’s World, n.d.) (Woods Hole Oceanographic Institution, n.d.).

AUG’s are specialized for long range and endurance. They use their special buoyancy and center of gravity changing mechanisms to propel themselves. This unique propulsion system decrease the energy consumption and increase the usage time to 6-12 months by creating a gliding motion. Depending on the model AUG’s change their buoyancy or weight actively to create vertical motion. This vertical motion is transformed to horizontal motion with passing flow over the wings that creates lift force. This motion is called as sawtooth motion. Commercially used AUG’s have approximately 5 kg payload capacity. This payload capacity is used for different types of sensors. Sensors can be changed according to user’s need. Changeable sensors create an opportunity for variety of data collection from water column. Collected data can be transferred via radio frequency or using the satellite. AUG’s can be controlled over a control center for receiving collected data and rearranging mission requirements after deployment.

### **1.1 Buoyancy Driven Underwater Gliders**

AUG’s are named after how they operate and have different name according to propulsion mechanism. Currently buoyancy driven underwater gliders are widely used

because of the robustness of the system. Autonomous underwater gliders are studied by Henry Stommel after the invention of the profiling floats. Stommel changed the autonomous profiling float design to investigate the open water and collect data from wide areas with great endurance (Rudnick, Davis, Eriksen, Fratantoni, & Perry, 2004). Most important advantage of buoyancy driven underwater gliders is the high endurance and covering range. Their operation time can reach up to 6-12 months depending on the working depth and selected sensors. Energy that is needed to operate the gliders comes from batteries (Jenkins & D'Spain, 2016). Main propulsion system depends on the buoyancy engine to reduce the energy consumption and preserve the high endurance. Vehicle change its buoyancy using hydraulic fluid or gas depending on the model. Fluid or gas is kept inside the vehicle in a tank. When the volume change is needed this fluid or gas is pumped to the flexible outer tank (external bladder) to increase the total volume of the vehicle to increase the buoyancy. Underwater gliders that use hydraulic oil in buoyancy system mostly use high pressure piston pumps because of their reliability and durability. Changing buoyancy creates a vertical motion. Therefore, it creates a flow over vehicle's wings with suitable angle of attack. This flow results in hydrodynamic lift and drag force for horizontal movement while ascending and descending (Davis, Eriksen, & Jones, 2002). These processes create a motion that called "sawtooth motion" as can be seen in Figure 1.3. One ascending and descending move is called yo. Thus, sawtooth trajectory is formed with repetition of yos.

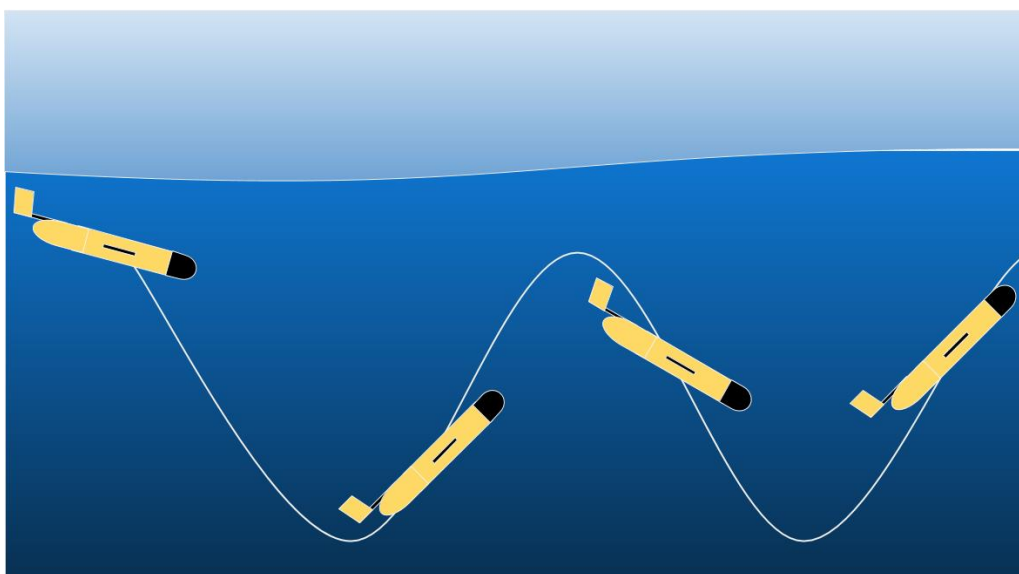


**Figure 1.3 :** Sawtooth motion of an underwater glider (IEEE Oceanic Engineering Society, n.d.).

Upward and downward movement that is created with the help of buoyancy mechanism needs to be controlled for precise motion. Underwater gliders move weight internally to create pitch. While creating pitch motion minimum movement of the weight is required to use minimum space. Designers solve this problem with using the heaviest object in the underwater glider's body which are battery packs that can reach up to 30% of the glider's total weight. Using a heavy object for pitch movement creates maximum moment for changing the position of the vehicle's nose and aft in minimum distance. While changing the buoyancy of the vehicle with the help of buoyancy mechanism, underwater gliders use moveable battery packs for changing the center of the gravity (Griffiths, Jones, Ferguson, & Bose, 2007). In addition to creating sawtooth motion with changing center of gravity, moveable battery packs are also used for pushing the antenna from the surface for communication operations. Communication position for most of the underwater gliders can be seen in Figure 1.4. Gathered data from sensor for navigation is processed by on-board computer to adjust the diving angle with battery packs with minimal movements (Bachmayer et al., 2004).



**Figure 1.4 :** Data transmitting and communication position of underwater glider (Autonomous Undersea Vehicle Applications Center, n.d.).

Controlling of the vehicles movement in the horizontal plane vary with the model of the underwater glider. Mostly 2 type of movement mechanism are used. First one is very effective, conventional rudder system. Rudder is coupled with magnets to decrease the chance of water leakage. Magnetic coupling is a robust and reliable

system as there is no moving part outside of the vehicle that remove the unreliability of the dynamic seals in excessive pressures. Second one is rotating the unsymmetrical battery pack to create intended roll motion for turning (Eriksen et al., 2001). When the gliders operating in shallow water maneuverability becomes an important factor. Reducing the turning radius decreases the chance of hitting underwater objects and increases the obstacle avoidance capabilities of the vehicle (Bender, Steinberg, Friedman, & Williams, 2006). This requirement unveils the importance of the maneuvering mechanisms.

Underwater gliders are surrounded with sensors for navigation and data gathering from the ocean. Autonomous system is dependent entirely on the sensors and navigational algorithms (Bender et al., 2006). Sensors that are used for navigation mainly inside a package that is called attitude sensing package. Attitude sensing package includes inertial measurement unit (IMU), inclinometer, three axis gyroscope, magnetometer, compass, pressure sensors and altimeter/sonar. Main purpose of this package is measuring the pitch, roll, heading and depth data of the vehicle to measure the speed and maintaining the route. On-board computer processes the data and control the propulsion system for navigating the vehicle to the given location. Heading values of the vehicle can be calculated with the data comes from IMU and magnetometer. The data comes from IMU and gyroscope is used for pitch and roll angles. Correction of the pitch and roll data combined with the heading values reduce the heading errors to less than  $1^\circ$  (Eriksen et al., 2001). Underwater gliders can record the depth values as well as the altitude values. Depth is important mostly for measuring the speed of the vehicle and scientific sensors to know where the data is collected. Altitude values are collected for understanding the distance to the ocean floor for safety. Protecting the vehicle from hitting the ocean floor or seamounts. Altimeter's range can be adjusted depending on the seabed material. GPS is another important part for navigation apart from the attitude sensor package. Underwater gliders get GPS data firstly after surfacing and lastly before diving. This algorithm used because of drifting with the wind and other effects while communicating with the control center. Last GPS data is used for navigating the vehicle to a desired location with the combination of attitude sensor package data.

Underwater gliders are mostly built in modular body to change scientific sensor payload easily with minor modifications as can be seen in Figure 1.5. Usage of the

underwater gliders increase the accuracy and the coverage of the oceanic models (Testor et al., 2011). Conductivity Temperature Depth (CTD), Acoustic Doppler Current Profiler (ADCP), Photosynthetically Active Radiation (PAR), Dissolved Oxygen (DO) sensor, pH sensor, Fluorometer / Backscatter / Turbidity sensors, Echo sounder and nitrate sensor can be adapted to the underwater gliders. Desired data can be collected from water column with the help of these low power, small size sensors (Kongberg Maritime, 2014). CTD is the most important sensor for underwater scientific research. It measures the conductivity of the water on chosen location combined with temperature and pressure data to obtain the value of the salinity. Salinity values later related with the depth values to create salinity profile of the water column. Salinity and temperature are main parameters for seawater density which directly affect the depth of the ocean surface mixed layer (Talley, 2002). ADCP is used for measuring how fast the water moves in the water column by using the sound wave principle called the Doppler effect (Kostaschuk, Best, Villard, Peakall, & Franklin, 2005). Sound waves have higher frequency while moving towards the observer than moving away. Sound wave that has constant frequency is transmitted by ADCP is called a ping. Pings that had been radiated from a moving away particle have decreased frequency when they came back to the receiver. The frequency difference between sent and received pings called Doppler shift. ADCP analyzes that Doppler shift to calculate how fast the particle is moving around. PAR sensor measure the light energy between 400 to 700 nanometers wavelengths which is absorbed by photosensitive pigments (Long, Rheuban, Berg, & Zieman, 2012). This parameter controls the primary production. Therefore it needs to be measured. Dissolved Oxygen sensor measures the dissolved oxygen level in water. Oxygen level is crucial for aquatic animals and organisms. Additionally gives information about the water quality. Turbidity sensor measure the light bounced back from the undissolved suspended matters in water column. This matter can be a mineral or organic like plankton. Turbidity level increases with increasing suspended solids. Measuring turbidity gives information about the water quality.



**Figure 1.5 :** Modular sensor payload section of an underwater glider (New Atlas, n.d.).

Collected data from mentioned sensors need to be transmitted to the control center for proper examination. Communication with the underwater glider also gives possibility of changing the route, location and requirements during the missions. Vehicle can connect periodically with the control center when it reaches to sea the surface. Underwater gliders use 3 types of communication system. These are RF, ARGOS (Advanced Research and Global Observation Satellite) and Iridium modem. RF is used for short range communication around 500m – 3 km depending on the line of sight. Radio frequency transmitters mostly used before the deployment to prepare the vehicle wirelessly. ARGOS and Iridium modems operate with satellite connection. These are the main communication systems for underwater gliders in open ocean. Iridium modem has relatively faster transfer rate and larger satellite coverage than ARGOS. Because of this Iridium modems are widely preferred.

## **1.2 Acoustics**

Acoustics is one of the subtopic of physics and engineering science that concentrates on sound and sound waves. Generation, propagation and reception of energy as vibrational waves are main subjects of acoustics (Bruneau, 2006). Shearing forces cannot be transmitted by fluids, in consequence of only inertia forces, fluids react against a change of shape. Change in fluid volume is concluded with change in its

pressure. Sound wave is created because of oscillatory disturbances that are caused by the energy travelling through the medium. Disturbance creates an oscillatory movement (vibration) in the molecules of the fluid with change in pressure, density and temperature that in response creates a sound wave (Jacobsen & Juhl, 2013). Changes in pressure are the signals that are heard by observer and detected by receiver as a sound. Vibrations of the particles in medium create a sound wave that is best described as longitudinal wave. When the direction of the fluid particles are parallel with the direction of the energy transport, longitudinal wave occurs. Peak pressure per cycle is represented by the amplitude of the sound wave. Therefore, higher amplitudes create louder and stronger sounds (Kellett, 2014).

The speed of sound varies with the elastic properties, density and temperature of the medium (Bohn, 1988). Elastic properties are different with different solids, fluids and gases. Elastic property is the resistance of a material to the deformation when a force exerted. Accepted speed of sound in air is around 340 m/s. However speed of sound calculation is more complex for underwater due to the effects of temperature, salinity, dissolved matters, hydrostatic pressure and density. Accepted speed of sound in underwater is mostly around 1500 m/s.

Propagation of the sound is affected by the frequency of the sound which is given in units of Hertz (Hz). Low frequency sound waves can travel extreme distance, and with increasing frequency sound attenuation increases. Travel distance of sound wave with different frequencies and wavelengths can be seen in Table 1.2.

**Table 1.2 :** Traveled distance for different frequencies and wavelengths (Kuperman, 2008).

Frequency	Wavelength	Distance
100 Hz	15 m	1000 km or more
1 kHz	1.5 m	100 km or more
10 kHz	15 cm	10 km
25 kHz	6 cm	3 km
50 kHz	3 cm	1 km
100 kHz	1.5 cm	600 m
500 kHz	3 mm	150 m
1 MHz	1.5 mm	50 m

Measured sound is specified as a magnitude called Sound Pressure Level (SPL) in unit of decibels (dB). Decibel is a nondimensional parameter that has a logarithmic scale. Decibel scale is used for describing the intensity of the sound. Intensity (I) is a vector quantity that gives amount of acoustic power per unit area in the direction of the flow with a scalar quantity. Intensity has the physical dimensional parameter that is power (watts) / area (m<sup>2</sup>). On the other hand Sound Intensity Level (SIL) is dimensionless parameter in unit of dB, which can be seen in Equation 1.1.

$$SIL = 10 \log_{10} \left( \frac{I}{I_{ref}} \right) \quad (1.1)$$

Reference intensity ( $I_{ref}$ ) is related with the threshold of human hearing which is 1E-12 W/m<sup>2</sup> in air at frequency of 1000 Hz. However reference intensity in water is 6.5E-19. I is the measured intensity.

Sound Pressure Level (SPL) logarithmic equation can be seen in Equation 1.2. Reference pressure value varies with the medium. Reference sound pressure value ( $P_{ref}$ ) in air is 20μPa, in water 1μPa.  $P_i$  is the measured sound pressure at specific frequency.

$$SPL = 20 \log_{10} \left( \frac{P_i}{P_{ref}} \right) \quad (1.2)$$

SPL is calculated in the range of frequencies and gives the dB level of the sound source or received dB level from a distance. Reaching out the only one dB in desired location is performed with the calculation of the Over All Sound Pressure Level (OASPL). Equation of the OASPL calculation (total dB) value from a receiver with whole set of frequencies can be seen in Equation 1.3.

$$OASPL = 20 \log_{10} \left( \sqrt{\sum_i \left( \frac{P_i}{P_{ref}} \right)^2} \right) \quad (1.3)$$

Another important concept about the sound pressure is the Loss of Transmission. Because of the absorption, reflection and dispersion, sound pressure (p) decreases with

the increasing distance ( $r$ ) from source ( $p \sim 1/r$ ). Reduction of the sound pressure is factor of 1 over the distance in ideal conditions. Sound Exposure Level (SEL) is also an important measure for a marine life research. SEL is used for comparison of the sounds in different types and exposure durations (André et al., 2009).

There are different type of acoustic sources. Important source types are;

- 0<sup>th</sup> order monopole
- 1<sup>st</sup> order dipole
- 2<sup>nd</sup> order quadrupole sources.

**Monopole sound source** is the most dominant type of source. The sound radiated from a monopole source is omnidirectional that arise from fluctuating mass injection or volume flow (Abom, 2010). Monopoles sources create sound waves that has much larger wavelengths than the dimensions of the source (Russell, Titlow, & Bemmen, 1999). Monopole sources can be exemplified as sound from a loudspeakers mounted in a box, exhaust pipe radiation, combustion and collapsing bubbles in fluids (cavitation). Illustration of the monopole source directivity pattern can be seen in Figure 1.6.

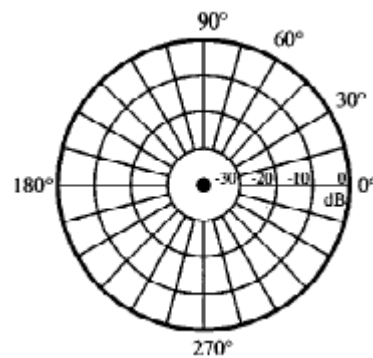


**Figure 1.6 :** Directivity pattern of monopole source (Russell et al., 1999).

**Dipole sound sources** represent fluctuating forces and momentums on the solid surface (Kellett, 2014). Dipole sound sources can be exemplified as a loudspeaker with no box and fluctuating forces that created from flow separations like sound created from a car antenna. Dipole sources have a cosine directional pattern as can be seen in Figure 1.7. Monopole and dipole sources only occur at boundary of the fluid.

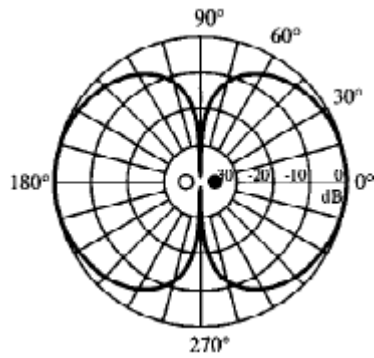


**Figure 1.7 :** Directivity pattern of dipole source (Russell et al., 1999).

Unsteady part of the momentum transportation in flow is produces a **quadrupole sound source** (Gustafsson, 2016). Sound that is radiated from a free turbulence in a fluid is an example for the quadrupole type volumetric sound source. Illustration of the quadrupole source directivity pattern can be seen in Figure 1.8.

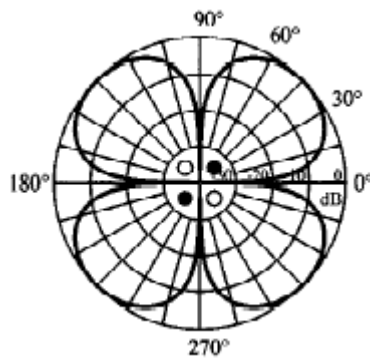


**Figure 1.8 :** Directivity pattern of quadrupole source (Russell et al., 1999).

### 1.2.1 Underwater acoustics

Underwater acoustics can be used for scientific, industrial and military purposes. Main usage areas of the acoustic in marine environment are ocean physics studies, marine geophysics, marine animal, earth history, oil and gas explorations, earthquake and volcano eruptions, navigation, communication, monitoring and defense studies (Ikpekha, 2017).

Measuring underwater sound and sound field in decibel requires a specific sensor that is called hydrophone which can withstand the corrosive effects, biofouling and high hydrostatic pressure of the deep oceans. Sound pressure is converted to an electrical voltage by the sensor (Creasey, 2003). Other important sensor for underwater research is SONAR (Sound Navigation and Ranging). SONARs use time interval between

transmitting and receiving sound waves to predict the size and shape of an object as well as the distance from the object.

One of the main study area of underwater acoustic's is the underwater ambient noise. In general, ambient noise means measured background noise level of a specific location. Sound Pressure Level of the point of interest is measured for analyzing the magnitude, effects and sources. Anthropogenic noise in the marine environment and effects are the key point for marine scientists (Dahl, Miller, Cato, & Andrew, 2008). Ambient noise is defined as "The noise associated with the background din emanating from a myriad of unidentified sources. Its distinguishing features are that it is due to multiple sources, individual sources are not identified (although the type of noise source-e.g., shipping, wind- may be known), and no one source dominates the received field" by National Research Council (National Research Council (US), 2003). Underwater ambient noise can be influenced by variety of sources as wind-sea noise, precipitation noise, shore/surf noise, beach profile, sediment transportation, aggregate extraction, commercial shipping, offshore industrial noise, military activity, sonar, aircraft noise, fishing activity, biological noise and thermal noise (Harland, Jones, & Clarke, 2005). Range of the ambient noise contributors can be seen in Figure 1.8 for different frequencies.

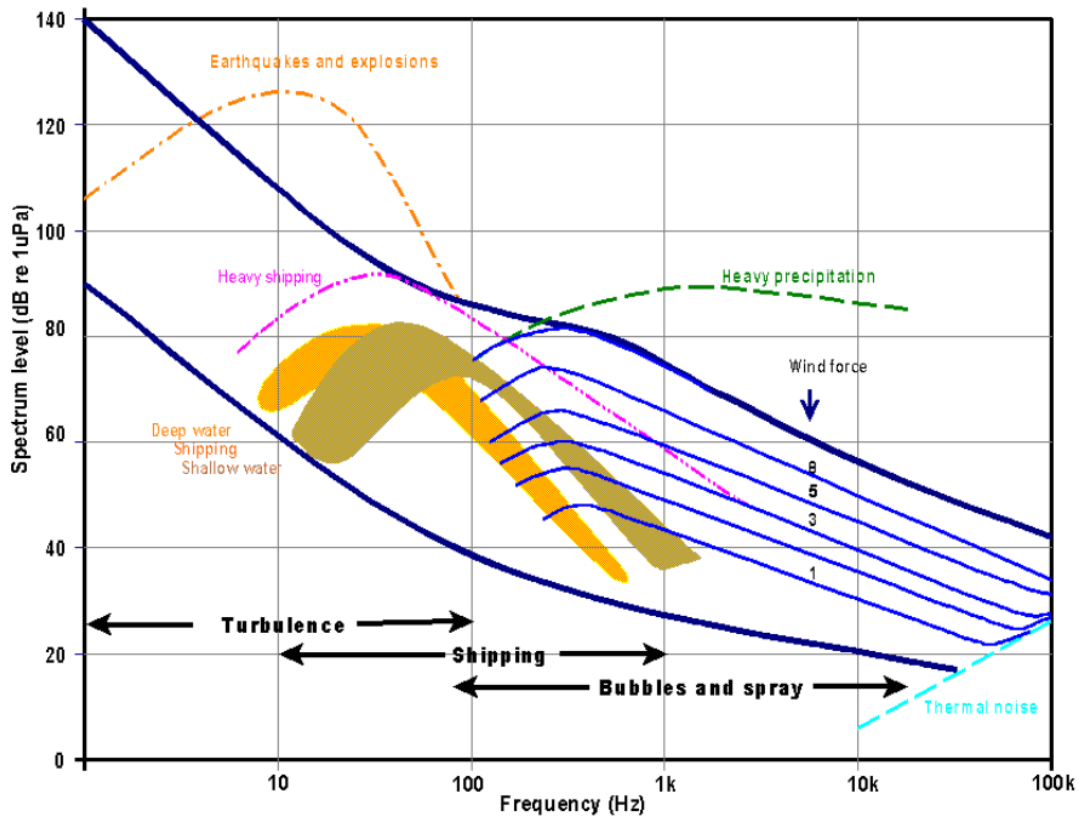


**Figure 1.9 :** Ambient noise spectra for different activities (Harland et al., 2005).

Describing the underwater radiated noise in the far field for an underwater or a surface vehicle needs to include several components. These noise sources can be categorized as flow induced noise (radiating through the hull), flow noise (hydrodynamic noise) and propeller noise. Induced noise is mostly produced by machinery and vibrations. Flow noise includes Turbulent Boundary Layer (TBL) excitation and cavity. Flow also creates vibration around the body and create a noise. Propeller noise depends on blade rate, blade modes and cavitation properties (Chevalier & Audoly, 2013).

### 1.2.2 Environmental effects and regulations of underwater noise

Excessive underwater noise exposure has crucial effects on marine animals which contains injury, hearing loss, behavioral changes, increasing stress, changes in neural system of the animal and in extreme cases even death (Popper et al., 2014). Different type of anthropogenic sounds affect the marine life in different ways due to the frequency and the intensity of the sound source. Possible effects of the different type of activity can be seen in Table 1.3.

**Table 1.3 :** Anthropogenic sound sources and possible effects (André et al., 2009).

Source	Effects
Ships	Masking Habitat displacement
Air guns (compressed air)	Masking Physical trauma Auditory loss Behavioral changes Habitat displacement Behavior conditioning effects
Intense low or mid frequency sonar activity	Physical trauma Auditory loss Behavioral change Behavior conditioning effects
Pile driving	Physical effects Auditory loss Behavioral change Behavior conditioning effects
Deepwater soundings, trawlers, fishing boats sonars	Masking Auditory loss Behavioral change Behavior conditioning effects
Dredgers	Behavioral change Habitat displacement Behavior conditioning effects
Drilling	Auditory loss Behavioral change Behavior conditioning effects
Towed fishing materials	Behavioral change Behavior conditioning effects Habitat displacement
Explosions	Physical trauma Auditory loss Behavioral change Behavior conditioning effects
Recreational boats	Masking Behavioral change Behavior conditioning effects
Acoustic hardware Airplanes	Behavior conditioning effects Behavior conditioning effects

Environmental effects of underwater noise is creating concern among the authorities. European Marine Strategy Framework Directive (MSFD) is increased the standard on good environmental status (GES) by adding the noise to anthropogenic sources in 2012 report (European Marine Strategy Framework Directive Good Environmental Status (MSFD-GES), 2012). The aim is to accomplish, maintain and continue to improve the good environmental status by 2020 and after 2020. Underwater noise and effects of total sound level on marine mammals will be discussed by intergovernmental cooperation involving Denmark, Estonia, Finland, Germany, Latvia, Lithuania, Poland, Russia, Sweden and the European Community in the Helsinki Commission (HELCOM) to preserve the health of marine animals health in the Baltic Sea. 15 European countries and the European Commission focused on possible effects of anthropogenic noise sources in OSPAR Commission recently. The Agreement on the Conservation of Small Cetaceans of the Baltic and North Seas (ASCOBANS) was signed to decrease the effects of underwater noise on small cetaceans. International Convention on Migratory Species was held for monitoring and studying the impacts of ambient noise with the participation of 116 countries (Erbe, 2013).

## **2. METHODS**

In this thesis, the underwater noise created by an underwater glider will be investigated using numerical modelling techniques. There are different methods to achieve the required noise data. Computational Fluid Dynamics (CFD) is the main tool for the calculations of the flow noise. Different techniques can be adapted to the CFD model to increase the accuracy of the data. Creating descend mesh for the case is the first step for the correct results and decreasing the computational time. Moreover, acoustic calculations depend on the chosen acoustic analogy. Compatible analogy need to be implemented for different cases.

### **2.1 Mesh**

Mesh can be explained as discreet visualization of the geometrical computation zone. CFD programs use triangle and quadrilateral cell shapes in two dimensional analysis. Three dimensional models use tetrahedron, quadrilateral pyramid, triangular prism and hexahedron elements. Sequence and connectivity of the cell change with the grid type. Three types of grid systems are mostly used. Structured grid has the regular connectivity. Unstructured grid has the irregular connectivity. The hybrid grid that is the combination of the unstructured and structured grids. Lines in these types of grids do not need to match at block boundaries.

Computational domain is the volume which physical parameters and experimental cases are solved with numerical methods. Computational domain size is an important parameter for correct results. Increasing domain size will increase the total cell number and computation time. However it could also decrease the error in the cases. Therefore, computational domain dimensions should be optimized to give minimum cell number with minimum error. This optimization is investigated with lots of works and analyses. These results need to be investigated for the best domain dimensions for specific cases. Setting refinement zones around the important flow zones will increase the accuracy of the case with decreasing cells number in those volumes. Refinement zone usage

create an opportunity to increase the accuracy of the case with minimal increase in total cell number and computation time.

Another important parameter for the accuracy of the results is boundary layer mesh. Number of prism layers, growth rate and total thickness of prism layer parameters are need to be set according to the used turbulence model and required  $y^+$  value.

## 2.2 CFD

Computational Fluid Dynamics (CFD) solve the velocity and pressure fields inside the control volume numerically using different algorithms to simulate the flow (Alobaid, 2018). CFD solves the Navier-Stokes Equations for describing the viscous flow with basic differential equations of fluid mechanics that are the equation of conservation of mass and conservation of momentum. Conservation of mass equation can be seen in Equation 2.1.

$$\frac{\partial \rho}{\partial t} + \nabla \cdot (\rho \vec{V}) = 0 \quad (2.1)$$

Conservation of the momentum equation's physical principle arises from the Newton's Second Law and the equation's in x-, y- and z- components can be seen in Equation 2.2, 2.3 and 2.4.

$$\rho \frac{Du}{Dt} = -\frac{\partial p}{\partial x} + \frac{\partial \tau_{xx}}{\partial x} + \frac{\partial \tau_{yx}}{\partial y} + \frac{\partial \tau_{zx}}{\partial z} + \rho f_x \quad (2.2)$$

$$\rho \frac{Dv}{Dt} = -\frac{\partial p}{\partial y} + \frac{\partial \tau_{xy}}{\partial x} + \frac{\partial \tau_{yy}}{\partial y} + \frac{\partial \tau_{zy}}{\partial z} + \rho f_y \quad (2.3)$$

$$\rho \frac{Dw}{Dt} = -\frac{\partial p}{\partial z} + \frac{\partial \tau_{xz}}{\partial x} + \frac{\partial \tau_{yz}}{\partial y} + \frac{\partial \tau_{zz}}{\partial z} + \rho f_z \quad (2.4)$$

Navier-Stokes Equations need to be solved to simulate the flow and turbulence in fluids. There are variety of the turbulence models to resolve all scales of the turbulence which there is not only one suitable model for all of the cases (Hart, 2016). Turbulence modelling change with the complexity of the model, required accuracy and the results. Different models can be chosen according to computational source, time and satisfying

the required results with best time management. Illustration of some available turbulence model comparisons can be seen in Figure 2.1

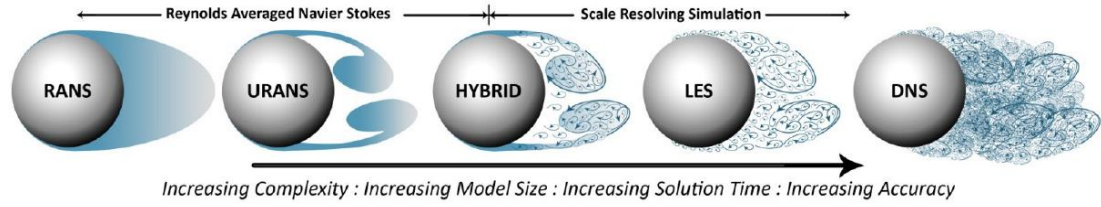


**Figure 2.1** : Comparison of the some turbulence models (Hart, 2016).

Direct Numerical Simulation (DNS) is used when solving the flow in detail and no simplifications or assumptions are made in this method. Therefore, it increases the solution time and requires significant amount of computational resources. Large Eddy Simulation (LES) uses filters for removing eddies which are small compared to the mesh resolution to decrease the computation time (Gustafsson, 2016). Reynolds Averaged Navier Stokes (RANS) was introduced and reduces the computational time significantly. RANS is the most commonly used turbulence model family. Attempt of describing the stress term in the RANS creates other turbulence models such as k-epsilon ( $k-\epsilon$ ) and k-omega ( $k-\omega$ ) (Sodja & Podgornik, 2007).

Another important parameter for the CFD and the turbulence models is the  $y^+$  which means nondimensional wall distance.  $y^+$  value indicates the coarseness or fineness of the mesh. Necessary  $y^+$  value varies with different turbulence models and turbulence models requirements for the cell size where are at near of the domain walls. It is important to choose proper  $y^+$  value for correct CFD results.  $y^+$  can be evaluated as a local Reynolds Number and can be calculated as Equation 2.5.

$$y^+ = \frac{yu_t}{\nu} \quad (2.5)$$

Where  $u_t$  is the friction velocity,  $y$  is the absolute distance from the wall and  $\nu$  is the kinematic viscosity. Friction velocity can be calculated as Equation 2.6.

$$u_t = \sqrt{\frac{\tau_\omega}{\rho}} \quad (2.6)$$

$\tau_w$  is the wall shear stress and can be calculated with the value of skin friction coefficient  $C_f$  as can be seen from Equation 2.7 and 2.8.

$$\tau_w = \frac{1}{2} C_f \rho U_\infty^2 \quad (2.7)$$

$$C_f = 0.0576 Re_d^{-\frac{1}{5}} \quad (2.8)$$

When the Reynolds Number is known  $y^+$  value can be calculated with following these steps that are shown above.

### 2.3 Aeroacoustic Methods

Aeroacoustic noise that is generated by fluids is a crucial parameter. Underwater vehicles, ships, helicopters, planes etc. create noise with the flow passing through a body. Turbine jet noise, noise that is generated from unsteady flow around wings, bodies and rotors, broadband noise that is occurred from boundary layer separation can be examples of the aerodynamic sound sources (Lyrintzis, 2003).

Prediction of the aeroacoustic sound source and magnitude of the sound becomes much easier with the numerical methods and increasing computational power that started a new field of Computational AeroAcoustics (CAA).

Acoustic field can be calculated through solving compressible Navier Stokes Equations directly. This method is called Direct CAA method. Sound generation, propagation and interaction between acoustic fields and flow fields can be computed with this method. Using this method increase the need of computational power because of the requirement of very small time steps and high mesh intensity. In consequence of solving acoustic domain and flow domain simultaneously, boundary need extra attention because of the artificial effects on the sound propagation (Gamage, 2017). Therefore, hybrid CAA methods are mostly preferred over direct methods.

Acoustic wave propagation in a fluid need to be explained before the explanation of the CAA methods. Propagation and the behavior of the wave in flow field is described by wave equation that is the form of rearranged Navier Stokes Equations. Homogeneous wave equation can be seen in Equation 2.9 where  $c_0$  is the speed of sound in fluid,  $p'$  is the fluctuation of pressure.

$$\left(\frac{1}{c_0^2} \frac{\partial^2}{\partial t^2} - \nabla^2\right) p' = 0 \quad (2.9)$$

When the right hand side of the acoustic wave equation is not equal to zero and equal to representation of the acoustic source nonhomogeneous wave equation appears as can be seen in Equation 2.10.

$$\left(\frac{1}{c_0^2} \frac{\partial^2}{\partial t^2} - \nabla^2\right) p' = f(\vec{x}, t) \quad (2.10)$$

Sir Michael James Lighthill was the first mathematician who introduced the first hybrid CAA method which was called Lighthill's Acoustic Analogy. Lighthill's aim was the estimation of the radiated sound from fluctuating fluid flows (Lighthill, 1952). Lighthill removed the external forces and heat sources from Navier Stokes equations and rearranged the nonhomogeneous wave equation as can be seen in Equation 2.11. Right hand side of the equation is sound source as in nonhomogeneous wave equation where  $\rho'$  is the density perturbation and  $T_{ij}$  is the Lighthill's stress tensor for a Newtonian fluid.

$$\frac{\partial^2 \rho'}{\partial t^2} - c_0^2 \frac{\partial^2 \rho'}{\partial x_i^2} = \frac{\partial^2 T_{ij}}{\partial x_i \partial x_j} \quad (2.11)$$

Right hand side of the Equation 2.11 (sound source) is divided into 3 components as explained before monopole ( $s_1$ ), dipole ( $s_2$ ) and quadrupole ( $s_3$ ) respectively  $s_1$ ,  $s_2$  and  $s_3$  as can be seen in Equation 2.12, 2.13 and 2.14.

$$s_1 = \frac{\partial}{\partial t} \left( m + \frac{1}{c_0^2} \frac{\partial}{\partial t} (p' - c_0^2 \rho') \right) \quad (2.12)$$

$$s_2 = \frac{\partial f_{v,i}}{\partial x_i} \quad (2.13)$$

$$s_3 = \frac{\partial^2}{\partial x_i \partial x_j} (\rho u_i u_j - \tau_{ij}) \quad (2.14)$$

Main restriction for the Lighthill's Acoustic Analogy is, conditions is not taken into account where there is a solid body inside the region. Lighthill considered only free radiation (Kaltenbacher, 2017). As a result, J. E. Ffowcs Williams and D. L. Hawkings considered additional source terms and extended the Lighthill's analogy when the flow interacts with moving or stationary solid surfaces in their 1969 paper. They created the Ffowcs Williams-Hawkings analogy (FW-H) (Williams & Hawkings, 1969). F-WH equation can be used in the cases where hydrodynamic noise generated by turbulent flow and rotating bodies such as propellers. Since FW-H analogy is a developed version of the Lighthill's analogy, all the assumptions are the same. These are; fluid has constant density, temperature and speed of sound is constant. The FW-H equation can be seen in Equation 2.15 where  $H(f)$  is the Heaviside function,  $\delta(f)$  represents the Dirac delta function,  $T_{ij}$  is Lighthill stress tensor,  $u$  is fluid velocity,  $v$  is body surface velocity,  $c$  is velocity of sound and  $n$  is normal vector that points into the fluid.

$$\begin{aligned} \frac{1}{c^2} \frac{\partial^2 p'(x, t)}{\partial t^2} - \nabla^2 p'(x, t) \\ = \frac{\partial}{\partial t} [(\rho_0 U_n) \delta(f)] - \frac{\partial}{\partial x_i} [L_i \delta(f)] + \frac{\partial^2}{\partial x_i \partial x_j} [T_{ij} H(f)] \end{aligned} \quad (2.15)$$

Where

$$U_i = [1 - (\rho/\rho_0)]v_i + (\rho u_i/\rho_0) \quad (2.16)$$

$$L_i = P_{ij} \hat{n}_j + \rho u_i (u_n - v_n) \quad (2.17)$$

$$T_{ij} = \rho u_i u_j + [(p - p_0) - c_0^2(\rho - \rho_0)]\delta_{ij} - \tau_{ij} \quad (2.18)$$

FW-H equation included sound source terms in Lighthill's equation that are named as loading noise, thickness noise and quadrupole noise. The quadrupole sound term is assumed to be negligible at low Mach number in most aerodynamic and hydrodynamic cases. However recent investigations showed that quadrupole term sources need to be taken into account that have significant contribution to the noise generation (Kellett, 2014). Thickness noise is caused by the volume displacement of the fluid and relative motion between body and the fluid that acts as a monopole sound source. Loading noise (lift noise) generated because of the pressure distribution over the surface and acts as a dipole sound source. These two terms are formed over a surface and sum of

these two terms is called the total surface noise. On the contrary quadrupole noise occurs in a volume.

In 1975, F. Farassat published a report and proposed a theory for the calculation of the acoustic pressure signature for arbitrary bodies in motion and the observer is not limited to the far field with extending FW-H equation (Farassat, 1975). F. Farassat and his colleagues at NASA Langley Research Center developed formulations that are called Formulation 1 (can be seen in Equation 2.19, 2.20 and 2.21) and Formulation 1A for the thickness and loading terms (Farassat, 2007). After these formulations F. Farassat and K. Brentner (2009) developed another formula for the quadrupole term which is similar to the thickness and loading terms in Formulation 1A that are called Formulation Q1 and Formulation Q1A.

$$p'(x, t) = p'_T(x, t) + p'_L(x, t) \quad (2.19)$$

$$p'_T(x, t) = \frac{1}{4\pi} \left( \int_{f=0} \left[ \frac{\rho_0(U_n + U_{\dot{n}})}{r(1 - M_r)^2} \right]_{ret} dS + \int_{f=0} \left[ \frac{\rho_0 U_n [rM_r + c(\dot{M}_r - M^2)]}{r^2(1 - M_r)^3} \right]_{ret} dS \right) \quad (2.20)$$

$$p'_L(x, t) = \frac{1}{4\pi} \left( \frac{1}{c} \int_{f=0} \left[ \frac{\dot{L}_r}{r(1 - M_r)^2} \right]_{ret} dS + \int_{f=0} \left[ \frac{(L_r - L_M)}{r^2(1 - M_r)^2} \right]_{ret} dS + \frac{1}{c} \int_{f=0} \left[ \frac{L_r [rM_r + c(M_r - M^2)]}{r^2(1 - M_r)^3} \right]_{ret} dS \right) \quad (2.21)$$

Where

$$M_i = \frac{v_i}{c} \quad (2.22)$$

$$U_i = v_i + \left( \frac{\rho}{\rho_0} \right) \left( \frac{u_i}{v_i} \right) \quad (2.23)$$

$$L_i = P_{ij} n_j + \left( \frac{\rho}{u_i} \right) \left( \frac{u_n}{v_n} \right) \quad (2.24)$$

These equations are valid for both the near and the far field calculations in the time domain.

Ffowcs Williams himself suggested the usage of a porous or permeable surface to capture the quadrupole sources effects. Adding permeable surface far from the body itself into model within the flow will contain the quadrupole sound sources within the integration surface. This means sources that arise from turbulence are captured with the help of porous surface.



### 3. VALIDATION

The validation case is comparison of DARPA Suboff total resistance to model results, as well as comparing acoustic results to other numerical acoustic result from the literature. Validation case is carried out in STAR-CCM+ software and mesh is created with the same software.

#### 3.1 Mesh

STAR-CCM+'s automated mesh tool is used for meshing for the models. Model's tip of the head is placed onto origin where is  $[0, 0, 0]$  on the coordinate system. Aft of the model stand in the positive x direction. Computational domain is chosen according to the experience in CFD and appropriate with the flow and case characteristics. Computational domain coordinates can be given with 2 corner coordinates that are  $[-7.5, -7.5, -7.5]$  and  $[20, 7.5, 7.5]$  in meters. Which means boundaries are 7.5 meters away in negative x direction, 20 meter away in positive x direction (to capture the wake zone), 7.5 meters away in positive and negative y direction and 7.5 meters away in positive and negative z direction from the tip of the head (origin). Inlet of the flow lies in negative x direction and outlet lies in positive x direction. Illustration of computational domain can be seen in Figure 3.1. Computational domain size was selected according to the model dimensions. Inlet of the domain's distance from the origin is  $1.72L$  where L is the models length. This number is attempted to keep over  $1.5L$ . Outlet of the domain's distance from the origin is chosen  $4.59L$  to increase the computation size in the wake zone.  $4.59L$  is selected for staying over the  $4L$  with rounding the cell size and using minimum cell that enough for simulation. Other dimensions of the computational domain are chosen same with the distance between the origin and the inlet.

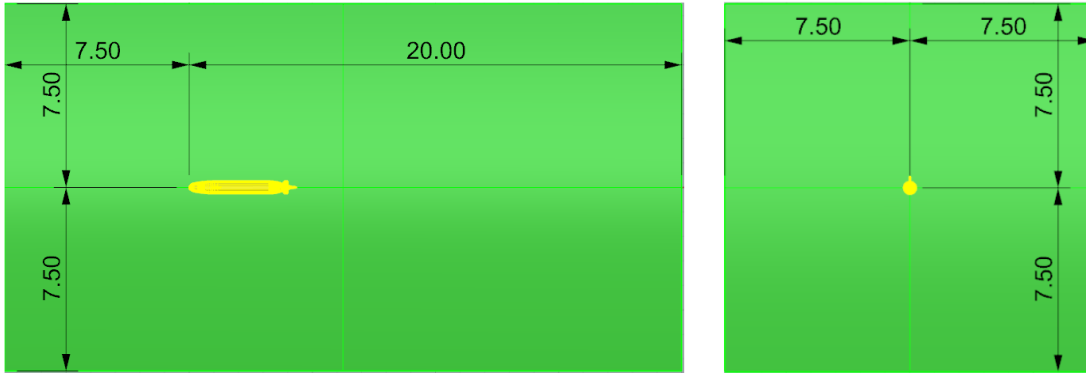


**Figure 3.1 :** Dimensions of the computational domain.

Refinement boxes are placed around the body where the computation requires better precision. These are the nearby regions of the body, the wake zone of the vehicle, the nearby regions of the sail and the rudder regions. Refinement regions shapes are varying depending on location. Nearby region of the body, wake zone and rudder region refinements have cylindrical shape while rudder region has rectangular prism shape. Cylindrical shape is chosen to reduce the mesh cell number. Cylinder refinement zone gives the same results with rectangular refinement zone with less cell in specific areas. These mesh refinement regions, computational domain mesh and growth of the mesh in boundary layer can be seen in Figures 3.2, 3.3, 3.4, 3.5 and 3.6. STAR-CCM+ automated mesh parameters are selected as Surface Remesher, Trimmed Cell Mesher and Prism Layer Mesher (boundary layer). Computational domain base size is selected 1.1 m to divide the domain in 25 pieces ( $27.5/1.1$ ). Base size in refinement zones is decreased to 2.5% of the domain base size around the body, 1.5% in wake zone, 1% around the rudder and sail to increase the mesh density in these zones.

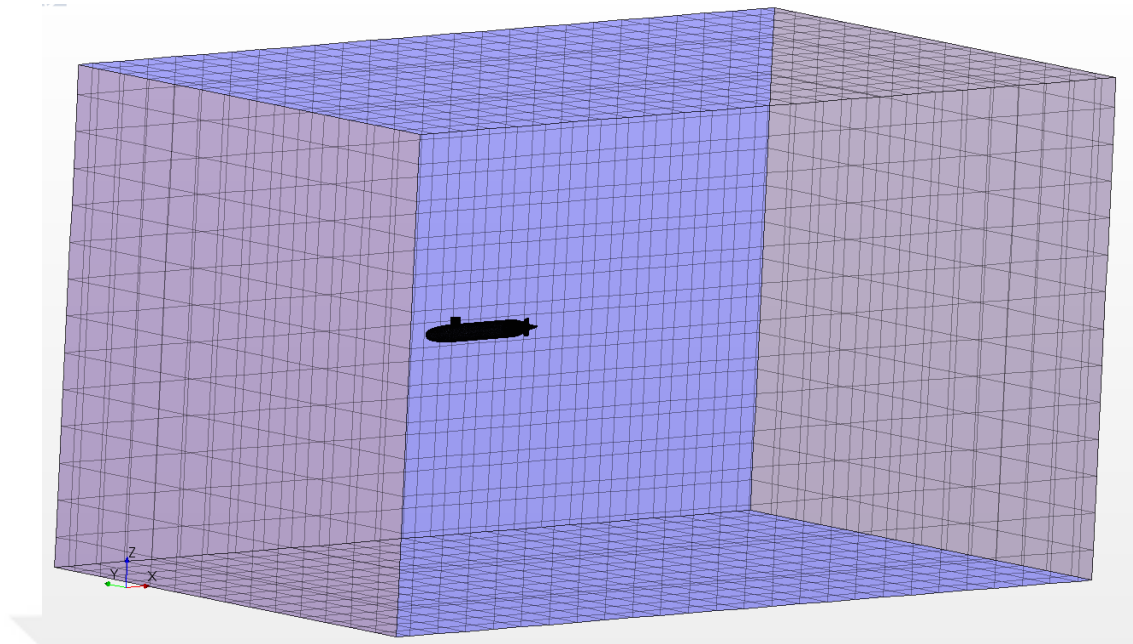


**Figure 3.2 :** Mesh domain.

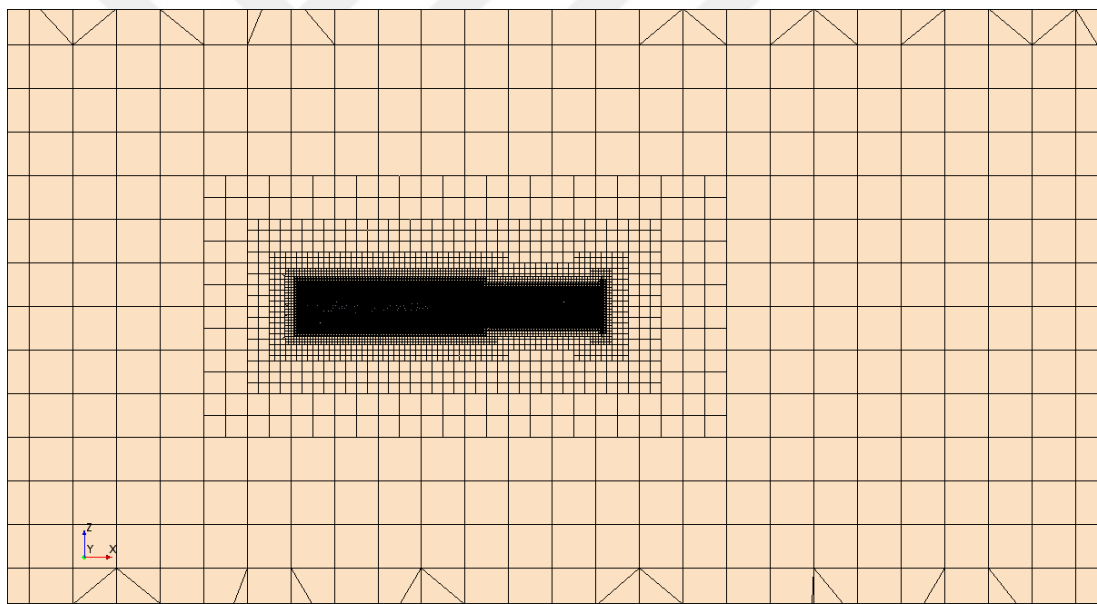


**Figure 3.3 :** Mesh inside of the domain.

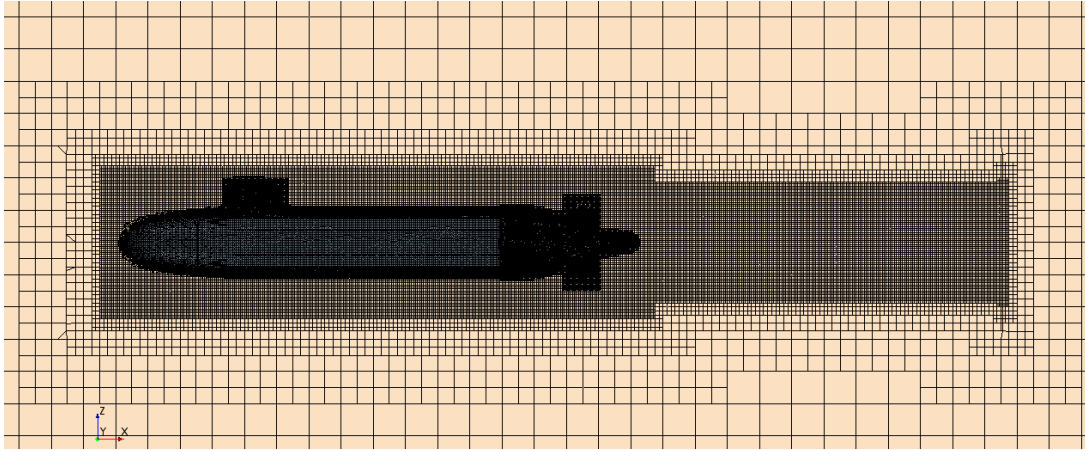


**Figure 3.4 :** Mesh of the domain and the refinement boxes.

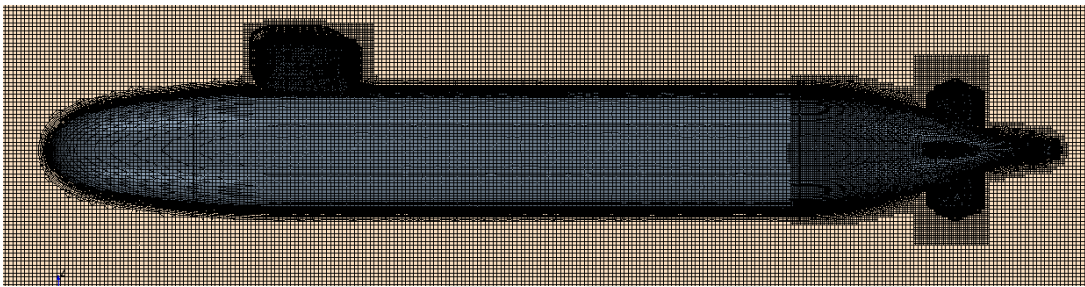


**Figure 3.5 :** Mesh around the body.

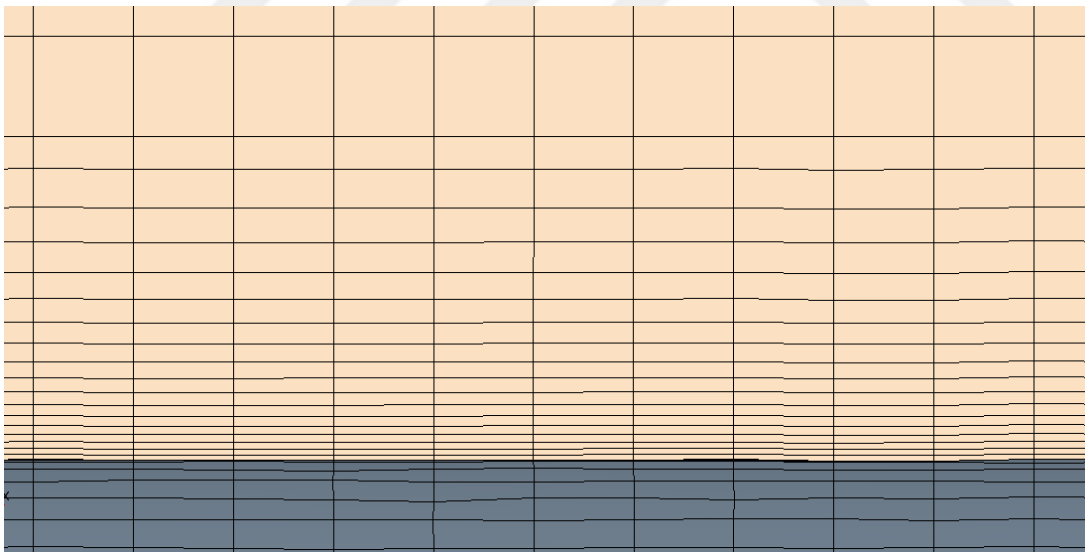


**Figure 3.6 :** Boundary layer.

K-epsilon ( $k-\epsilon$ ) turbulence model is selected for the simulation with RANS (Reynolds Averaged Navier Stokes) simulation type. K-epsilon is well suited where  $y^+$  value around 50 in the boundary layer. That is the selected value for the case because of the mesh properties. Using RANS decreases the computational time substantially. Total number of cells are 3.6M after these arrangements. Resistance comparison are done

with the experiment results to verify the mesh quality and difference between CFD and experiments are tabulated in Table 3.1 which are close for verifying the mesh.

### 3.2 Resistance

Validation of the CFD setup and results that are carried out with the STAR-CCM+ is compared with the well-known form and case of DARPA Suboff experiments. DARPA Suboff model used with full appendages without propeller as can be seen in Figure 3.7. DARPA Suboff hull has 4.356 m length and 0.508 m diameter. Fore body length is 1.016 m, parallel body section is 1.111 m and after body's length is 0.095 m (Groves, Huang, & Chang, 1989). Comparison of the results are carried out with the DARPA Suboff Configuration 8 (Hull with sail and four stern appendages) and Stern Configuration 3 as stated in the experimental data by (Liu & Huang, 1998). 5.93 knots (3.05 m/s) is chosen as the speed for comparison. Reynolds number of the Suboff model is  $1.3E07$ .

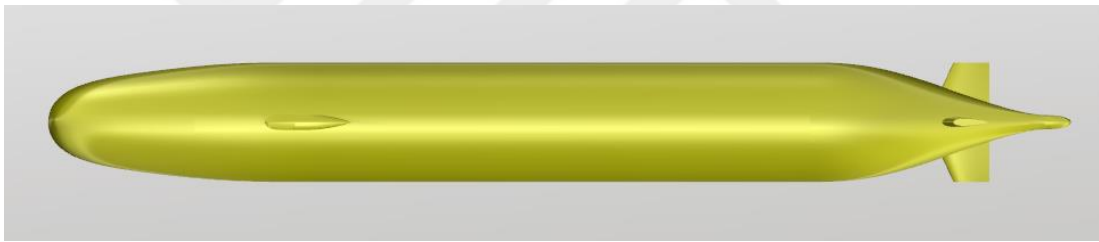


**Figure 3.7 :** Top view of DARPA Suboff model.

Validation is started with the resistance data of the model with the Liu & Huang (1998) experimental study. Results and parameters can be seen in Table 3.1.

**Table 3.1 :** Comparison of the CFD results with the experiment

Model Speed [m/s]	Total Resistance (CFD) [N]	Total Resistance (Experiment) [N]	Relative Error [%]
3.05	100.82	102.3	1.45

CFD simulation resistance results are relatively accurate with the given data in Table 3.1.

### 3.3 CFD Parameters and Flow Noise

Simulation is started in steady state condition to decrease the computation time. Implicit unsteady state is started after simulation accuracy was verified and total resistance value has converged. Steady state solution results are used as initial condition for unsteady state.

Incompressible flow (constant density) assumption is made throughout the simulation. Density was chosen  $998.2 \text{ kg/m}^3$  for the fluid with the kinematic viscosity of  $1.00481\text{E-}06 \text{ m}^2/\text{s}$ . Newtonian transport model is used in simulation.

Time step of the simulation is selected  $5 \times 10^{-5}$  seconds to capture the frequency range from 0 to 10000 Hertz. This time step value and mesh properties gives convective Courant Number less than 3. Inner iteration number for the simulation is chosen 5. Case of the DARPA Suboff model had run for 6000 iterations in steady state until the resistance value has converged. Unsteady simulation was run for 111000 iterations up to the physical time of 1.06 s.

Validation of the sound pressure levels of the model start with the locating virtual hydrophones. Virtual hydrophones are located as (H. Yao, Zhang, Liu, & Jiang, 2017) X1 and X11 points are used because of the given values and figures. X in the names of the points indicates elongation direction in coordinate system and the numbers are selected in numerical order with changing distance by the authors. X1 and X11 virtual hydrophones locations can be seen in Table 3.2.

**Table 3.2 :** Virtual hydrophones locations.

Virtual Hydrophone	Coordinate [m]
X1	[4.36,0,0]
X11	[12.00,0,0]

The flow noise of the DARPA Suboff with Configuration 8 in 3.05 m/s speed is compared with the (H. Yao et al., 2017) Boundary Element Method (BEM) results by solving the FW-H equations. StarCcm+ is used for predicting the acoustic values. Firstly, noise is predicted in the time domain. Results are taken in the form of pressure time series. Calculation of the underwater radiated noise is carried out with the Fast Fourier Transform (FFT). FFT converts the time domain acoustic data that was collected throughout the simulation to the frequency domain. Time interval of the FFT

is chosen according to the flow properties and convergence. A discrete probability function is applied to the FFT data. Hann Function is used as a window function. Choosing time step  $5E-5$  gives up to 10000 Hertz in spectral data. Calculated spectra of the flow noise of the DARPA Suboff with FW-H using StarCcm+ can be seen in Figure 3.8.

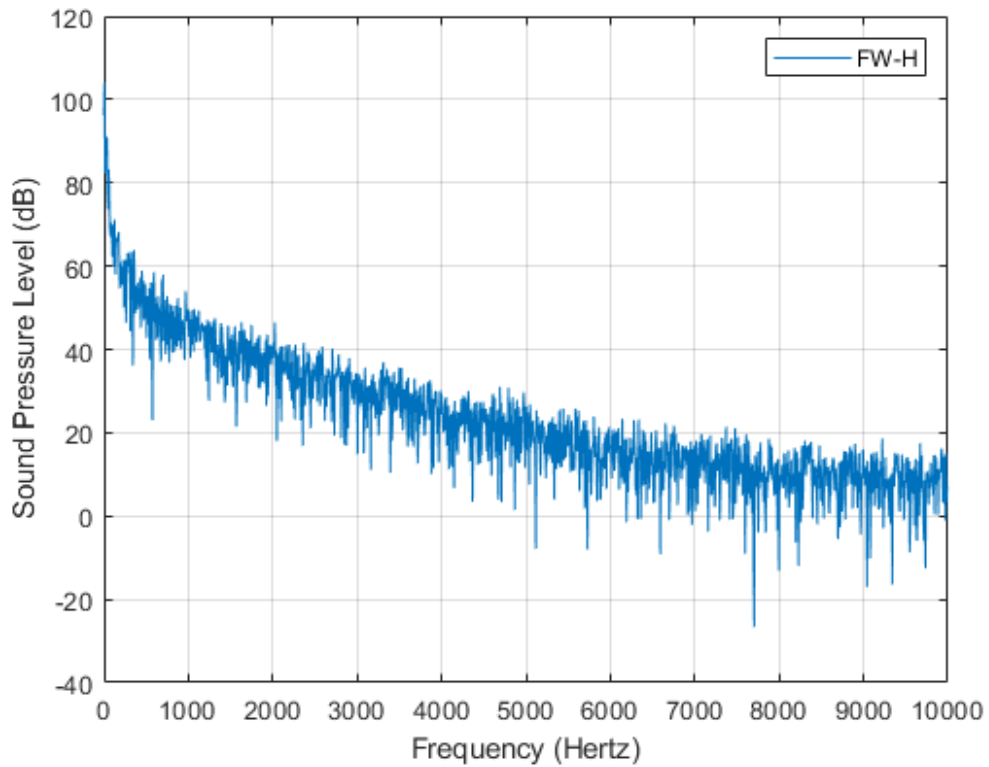


**Figure 3.8 :** Calculated DARPA Suboff sound pressure levels to the 10 kH.

Comparison of the sound pressure levels that was calculated with BEM, FW-H (H. Yao et al., 2017) and FW-H at the virtual hydrophone X1 location can be seen in Figure 3.9.

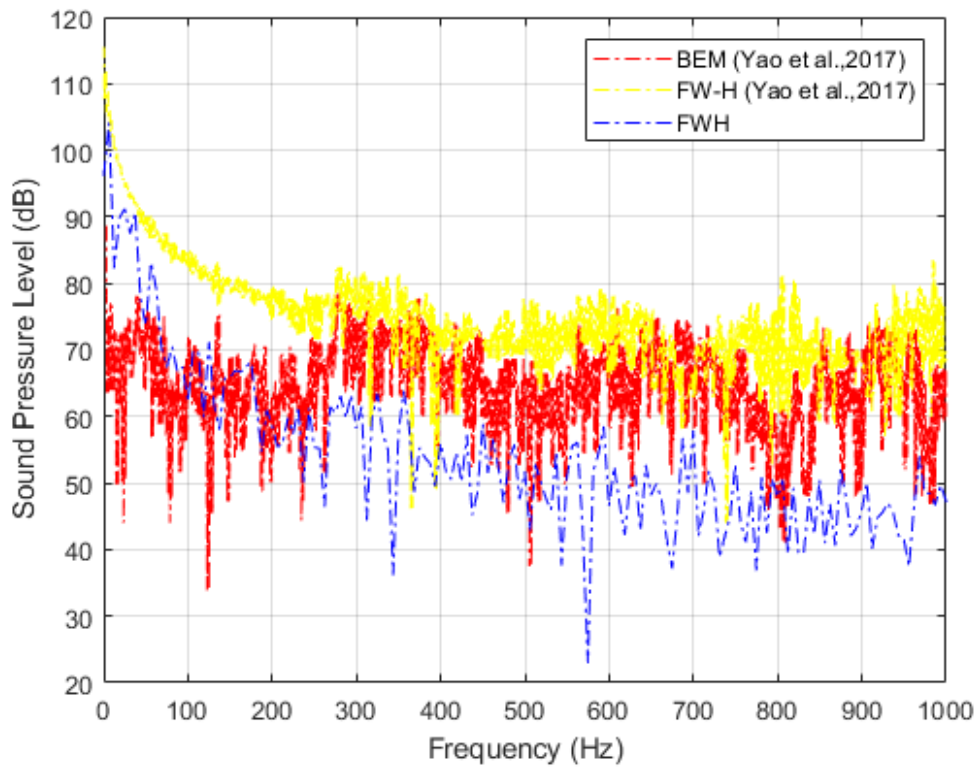


**Figure 3.9 :** Comparison of the methods to the 1000 Hz.

Spectra of the flow noise of the virtual hydrophone X11 point to the 1000 Hertz can be seen in Figure 3.10.

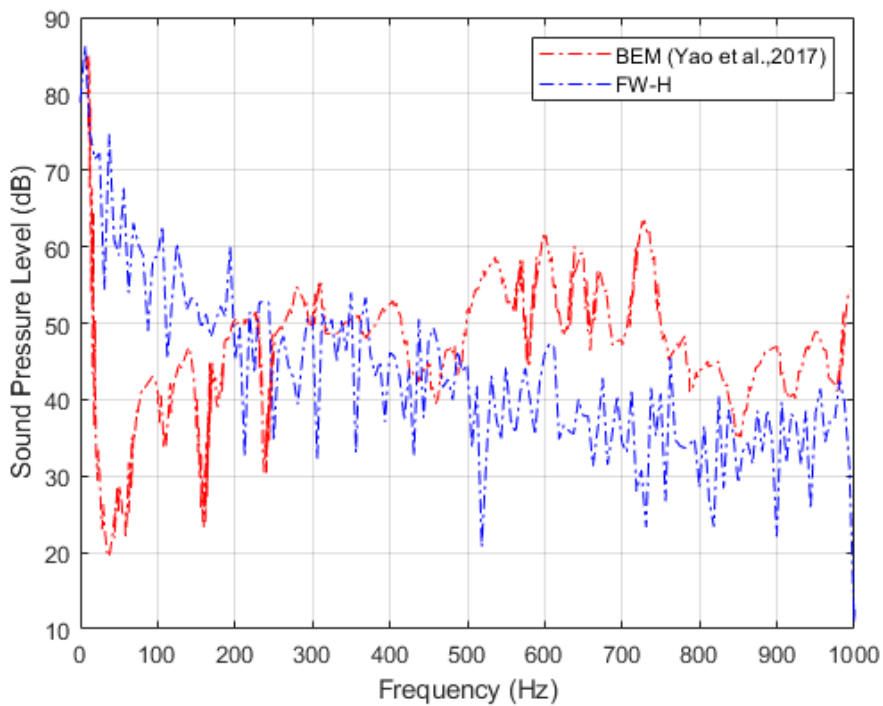


**Figure 3.10 :** Flow noise spectra comparison in Point X11.

Figure 3.9 and Figure 3.10 show that both analysis have close peaks but STAR-CCM+ FW-H analysis has lower values in some frequencies. However, we are more interested in the Over All Sound Pressure Level (OASPL) as it is a more crucial parameter. Comparison of the Over All Sound Pressure Levels gives the main estimation about the sound around the point. Calculation of the OASPL for the DARPA Suboff in experiment gives 101.3 dB value (S. Yao, Guang, & Gao, 2013) (Lu, Zhang, & Pan, 2008) (Zhang, Fan, & Sun, 2007). Calculated value of the OASPL throughout the simulation in STAR-CCM+ is 105.1 dB. This value proves that numerical simulation can be used for the investigation of the radiated noise in characteristic points and gives close results to the experiment.





## 4. UNDERWATER GLIDER MODELLING

### 4.1 Model, Mesh and CFD

After the completion of the validation models with the DARPA Suboff, underwater glider modelling is started. StarCcm+ CFD software is used throughout the model preparation. One of the commercial underwater glider design is used for the model (Narval R&D). Model of the underwater glider from side can be seen in Figure 4.1, top view of the model can be seen in Figure 4.2.

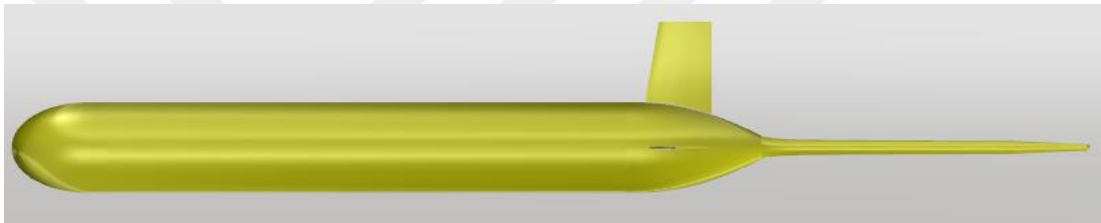


**Figure 4.1 :** Side view of the underwater glider.

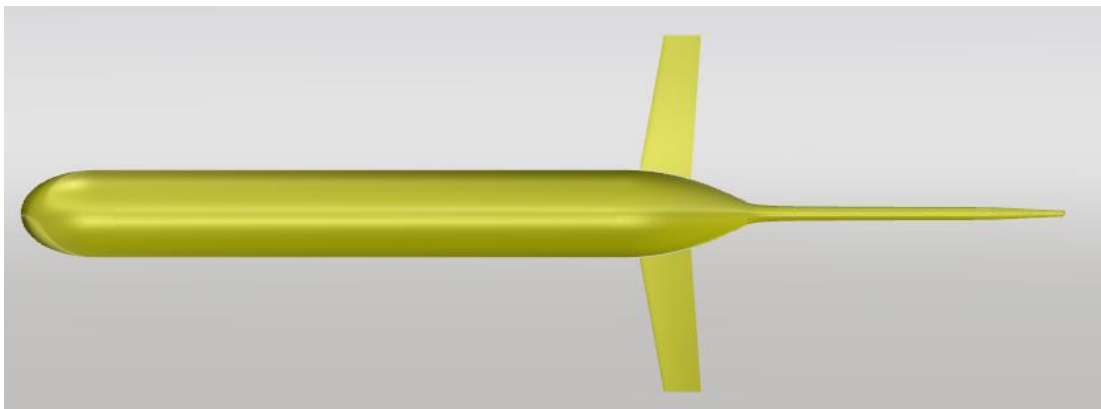


**Figure 4.2 :** Top view of the underwater glider.

3 cases are run for the comparison of the radiated noise of underwater glider in different attack angles. Attack angles selected for the cases are  $-10^\circ$ ,  $0^\circ$ ,  $10^\circ$ . Model of the underwater glider in  $0^\circ$  attack angle is placed on the coordinate system where the tip of the head is on  $[0, 0, 0]$  (origin). Antenna of the vehicle lies in positive x direction and the tip of the rudder lies in positive y direction. Total length of the model without antenna is 1970 mm, with antenna is 2834 mm (L). Hull diameter of the vehicle (D) is

240 mm with wing span of 966 mm. Tip of the rudder's distance from origin in positive y direction is 328 mm.

Inlet of the computational domain lies in negative x, outlet lies in positive x direction. The box that creates computational domain 2 corner coordinates are [-5, -5, -5] and [13, 5, 5]. Inlet of the computational domain lies 1.76L away from the origin which is larger than the minimum requirement of 1.5L. Outlet of the domain lies 4.59L away from the origin to increase the size of the domain at the back to analyze wake zone in bigger volume which is larger than 4L. Other dimensions of the domain (in y and z direction) is chosen same with the distance between inlet and the origin. Dimensions of the computational domain for the underwater glider can be seen in Figure 4.3.

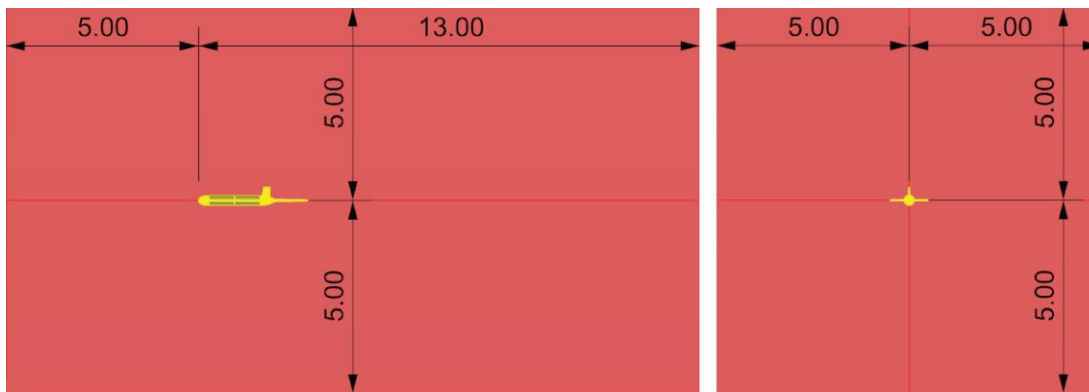


**Figure 4.3 :** Computational domain dimensions of the underwater glider.

Refinement boxes and cylinder are placed where the precision needed for the computation. Refinement zones locations are selected as close as the validation case where are around the body and the wake zone, the nearby region of the wings and the rudder region and additionally antenna region. Meshes of the underwater glider cases at  $0^\circ$ ,  $+10^\circ$  and  $-10^\circ$  attack angles can be seen in Figure 4.4, 4.5, 4.6, 4.7, 4.8, 4.9 and 4.10. Underwater glider is rotated from point of [1, 0, 0] for appropriate comparison of the virtual hydrophone at angle of attack  $+10^\circ$  and  $-10^\circ$ .

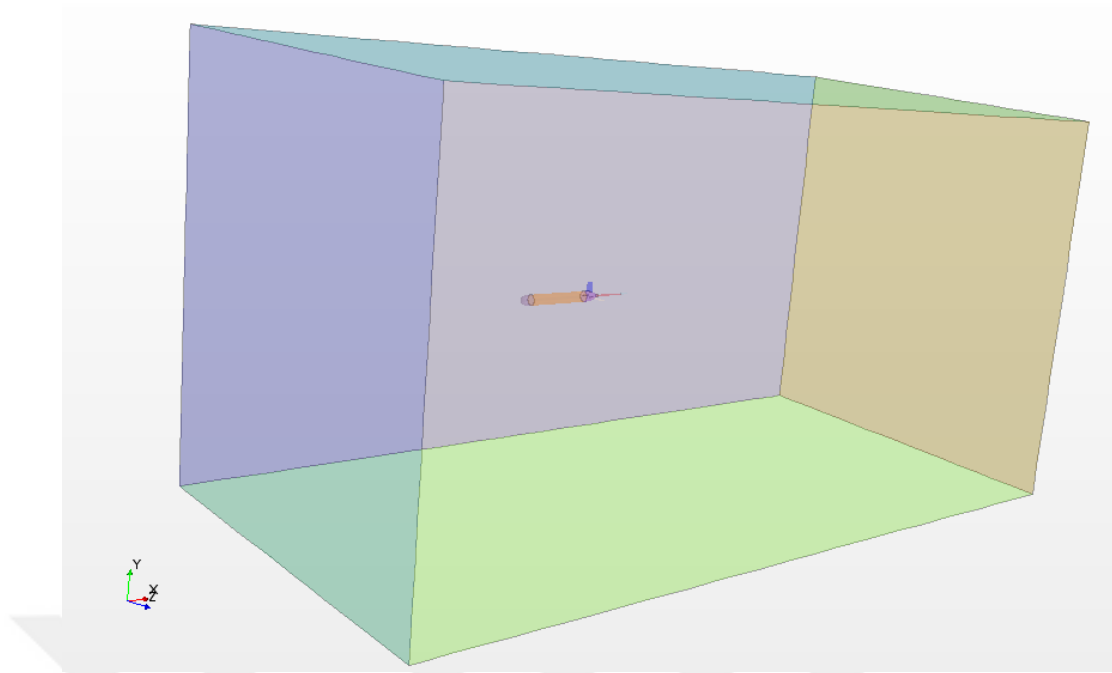


**Figure 4.4 :** Domain of the underwater glider case and location.

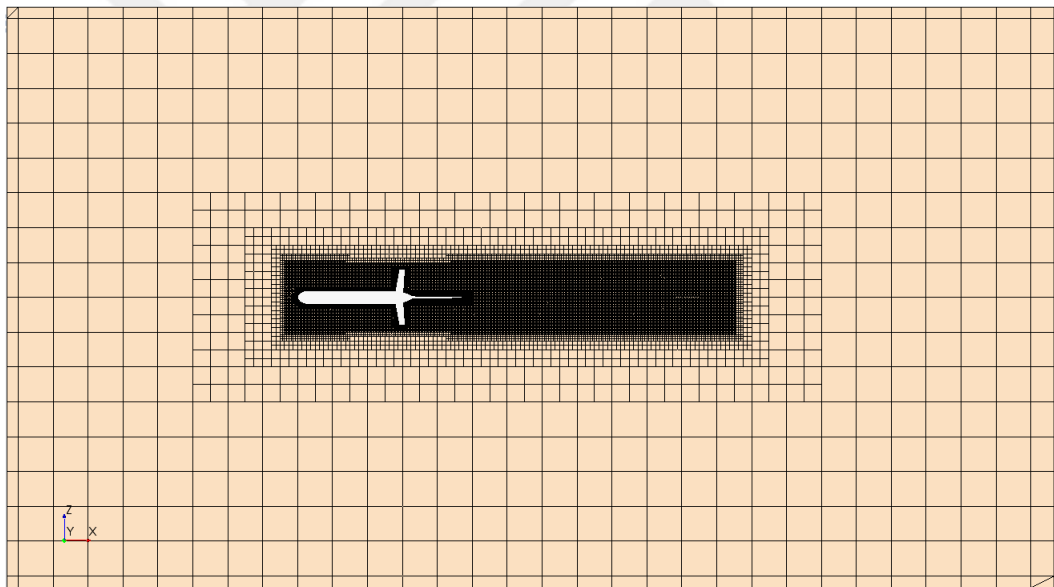


**Figure 4.5 :** Mesh inside of the domain for underwater glider case.

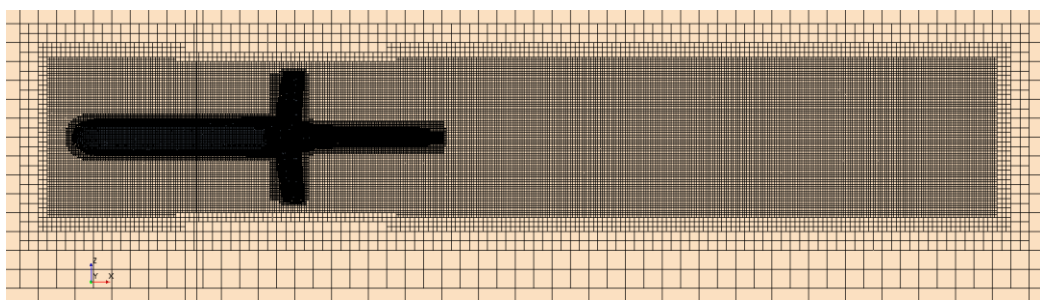


**Figure 4.6 :** Mesh of the refinement zones and surface from top.

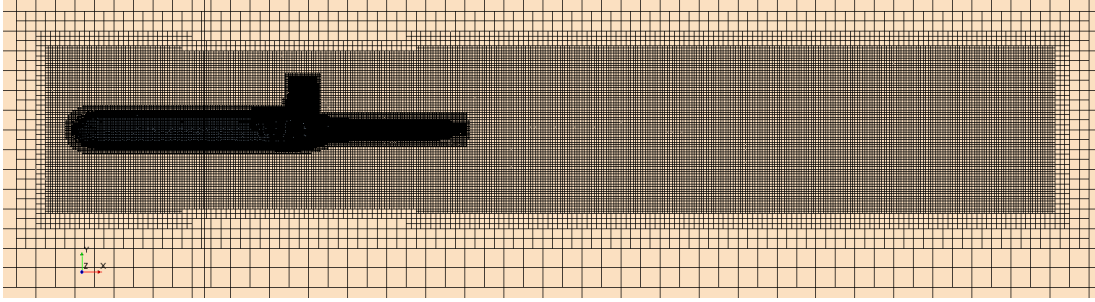


**Figure 4.7 :** Mesh of the refinement zones and surface from side.

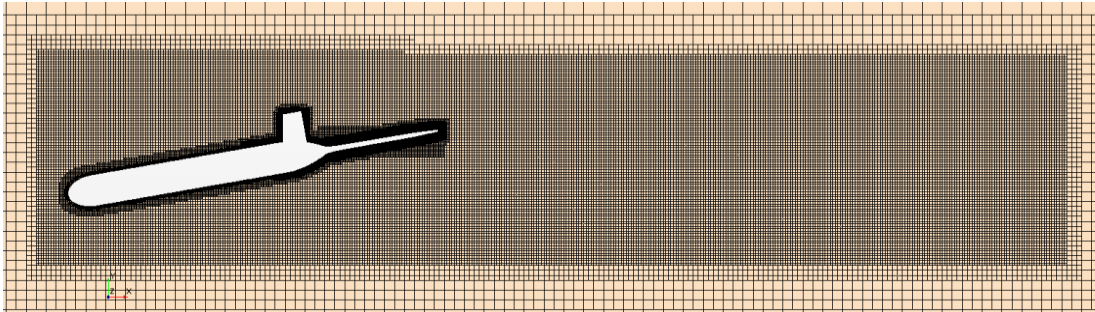


**Figure 4.8 :** Mesh of the refinement zones from side for +10° angle of attack.

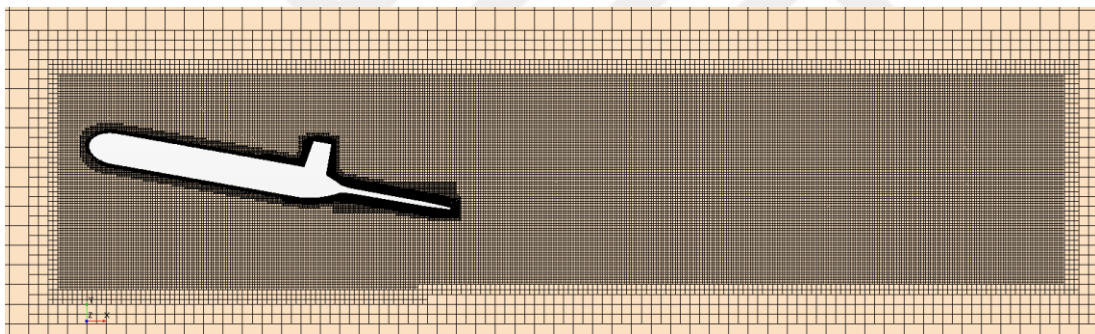


**Figure 4.9 :** Mesh of the refinement zones from side for -10° angle of attack.

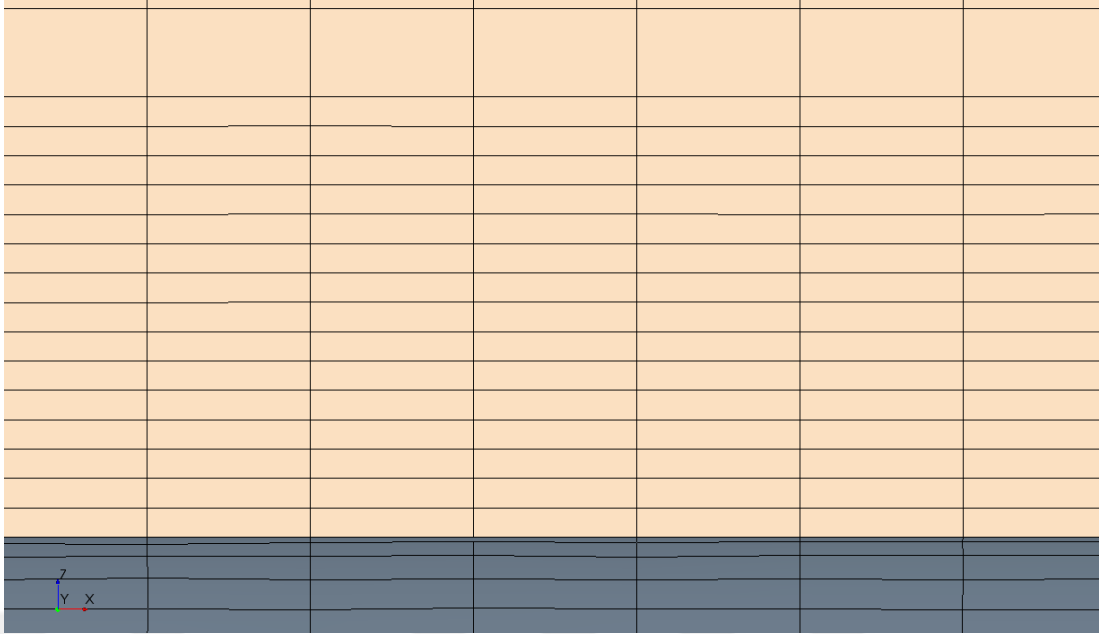


**Figure 4.10 :** Boundary layer of underwater glider case for  $0^\circ$  angle of attack.

Turbulence model,  $y^+$  value and other CFD parameters are selected same as validation case in all underwater glider cases. K-epsilon ( $k-\epsilon$ ) turbulence model of the URANS family is used.  $y^+$  value is set around 50 in the boundary layer. STAR-CCM+ automated mesh mesher is used for creating the mesh zones. Mesh parameters are selected as Surface Remesher, Trimmed Cell Mesher and Prism Layer Mesher. Base size of the computational domain is selected 0.6 m that is different value from validation case to increase the division of the computational domain. Base of the domain is divided into 30 pieces ( $18\text{m} / 0.6\text{m}$ ). Base size in refinement zones is decreased 1.5625 % of the base size in antenna refinement zone, 3.125 % around the body and in the wake zone, 0.78125 % in the rudder zone and 1.5625 % around the wings for all cases. However refinement zones dimensions are selected different to cover all the parts after the rotation and keeping these zones parallel to the flow. Minimum dimensions are tried to be selected without affecting the computation results. As a result of these arrangements total cell number for the case at  $0^\circ$  angle of attack is become 3.7M, for  $+10^\circ$  and  $-10^\circ$  angle of attack cases is become 4.8M.

Constant density assumption is made with the fluid density  $998.2 \text{ kg/m}^3$  and dynamic viscosity  $0.001003 \text{ Pa}\cdot\text{s}$ . Fluid selected as Newtonian fluid. Flow velocity is selected 1 m/s in positive x direction. Calculation with these parameters shows that Reynolds Number for the cases is  $2.8\text{E}6$ .

Time step of the simulation is selected same as validation case that is 5E-5 to increase the frequency range up to 10000 Hertz for and inner iteration of the calculation is selected as 5 for all cases. Convective Courant Number is kept below 2.2.

## 4.2 Virtual Hydrophones

Virtual hydrophone locations are selected according to the calculations with the first case of underwater glider that is the attack angle  $0^\circ$  and validation case with DARPA Suboff. Virtual hydrophones locations can be categorized as 2 groups and subcategorized to the closeness of the vehicle parts. First group of hydrophones are located near the body and extended through the x, y and z direction. Because of the symmetry in XY plane hydrophones lies in z direction elongate only to the positive z side. Second group of hydrophones are placed to create a volume that is formed by virtual hydrophones. Creating volume at the back of the vehicle will improve the comparison quality and change in the noise in both near and far field can be observed with different attack angles. Volume that is formed by hydrophones 2 corners coordinates are selected as [3, -1, 0] and [8, 1, 1]. Volume is divided with 0.5 m intervals in x direction, 0.4 m intervals in y direction and 0.2 m intervals in z direction. This process create 396 virtual hydrophones in the volume. Hydrophones are named after the closeness to the part of the vehicle, elongation and distance from the origin in that direction.

Virtual hydrophone volume is created after the results of the case of attack angle  $0^\circ$ . Results are analyzed and locations of the peaks and rapid changes are kept inside of this volume. Locations of the hydrophones of the first group for  $0^\circ$  angle of attack case can be seen in Table 4.1, also visualization of these hydrophones that are shown as red dots for the  $0^\circ$  angle of attack case can be seen in Figure 4.11.

**Table 4.1 :** Virtual hydrophones coordinates for  $0^\circ$  attack angle case.

Virtual Hydrophones Name	x coordinate [m]	y coordinate [m]	z coordinate [m]	Group Definition
X3	3	0	0	Xx
X4	4	0	0	Xx
X5	5	0	0	Xx
X-0.5	-0.5	0	0	Xx
X0	0	0	0	Xx
X2.9	2.9	0	0	Xx
X2.84	2.84	0	0	Xx

**Table 4.1 (continued) : Virtual hydrophones coordinates for 0° attack angle case.**

Virtual Hydrophones Name	x coordinate [m]	y coordinate [m]	z coordinate [m]	Group Definition
X2.85	2.85	0	0	Xx
X.86	2.86	0	0	Xx
X6	6	0	0	Xx
X8	8	0	0	Xx
X10	10	0	0	Xx
Wing_X1.9	1.9	0	0.484	Wing_Xx
Wing_X1.85	1.85	0	0.484	Wing_Xx
Wing_X2	2	0	0.484	Wing_Xx
Wing_X2.5	2.5	0	0.484	Wing_Xx
Wing_X2.05	2.05	0	0.484	Wing_Xx
Wing_X2.25	2.25	0	0.484	Wing_Xx
Wing_X3	3	0	0.484	Wing_Xx
Wing_Z0.1	1.85	0	0.1	Wing_Zx
Wing_Z0.2	1.85	0	0.2	Wing_Zx
Wing_Z0.3	1.85	0	0.3	Wing_Zx
Wing_Z0.4	1.85	0	0.4	Wing_Zx
Wing_Z0.09	1.85	0	0.09	Wing_Zx
Wing_2_Z0.1	1.9	0	0.1	Wing_2_Zx
Wing_2_Z0.2	1.9	0	0.2	Wing_2_Zx
Wing_2_Z0.3	1.9	0	0.3	Wing_2_Zx
Wing_2_Z0.4	1.9	0	0.4	Wing_2_Zx
Wing_2_Z0.07	1.9	0	0.07	Wing_2_Zx
Wing_2_Z0.09	1.9	0	0.09	Wing_2_Zx
Rudder_X1.9	1.9	0.328	0	Rudder_Xx
Rudder_X1.85	1.85	0.328	0	Rudder_Xx
Rudder_X1.86	1.86	0.328	0	Rudder_Xx
Rudder_X1.87	1.87	0.328	0	Rudder_Xx
Rudder_X1.95	1.95	0.328	0	Rudder_Xx
Rudder_X2	2	0.328	0	Rudder_Xx
Rudder_X2.5	2.5	0.328	0	Rudder_Xx
Rudder_X2.85	2.85	0.328	0	Rudder_Xx
Rudder_X3	3	0.328	0	Rudder_Xx
Rudder_X4	4	0.328	0	Rudder_Xx
Rudder_X5	5	0.328	0	Rudder_Xx
Rudder_X6	6	0.328	0	Rudder_Xx
Rudder_X8	8	0.328	0	Rudder_Xx
Rudder_X10	10	0.328	0	Rudder_Xx
Rudder_2_Y0.1	1.9	0.1	0	Rudder_2_Yx
Rudder_2_Y0.2	1.9	0.2	0	Rudder_2_Yx
Rudder_2_Y0.3	1.9	0.3	0	Rudder_2_Yx
Rudder_2_Y0.07	1.9	0.07	0	Rudder_2_Yx
Rudder_2_Y0.08	1.9	0.08	0	Rudder_2_Yx
Rudder_2_Y0.15	1.9	0.15	0	Rudder_2_Yx

**Table 4.1 (continued) :** Virtual hydrophones coordinates for 0° attack angle case.

Virtual Hydrophones Name	x coordinate [m]	y coordinate [m]	z coordinate [m]	Group Definition
Hull_Y-0.12	1	-0.12	0	Hull
Hull_Y0.12	1	0.12	0	Hull
Hull_Z-0.12	1	0	-0.12	Hull
Hull_Z0.12	1	0	0.12	Hull
Back_X3_Y1	3	1	0	Back
Back_X3_Z1	3	0	1	Back
Antenna_X2	2	0	0.028	Antenna_Xx
Antenna_X2.5	2.5	0	0.028	Antenna_Xx
Antenna_X2.05	2.05	0	0.028	Antenna_Xx
Antenna_X2.25	2.25	0	0.028	Antenna_Xx
Antenna_X2.75	2.75	0	0.028	Antenna_Xx
Antenna_X3	3	0	0.028	Antenna_Xx
Rudder_Y0.1	1.85	0.1	0	Rudder_Yx
Rudder_Y0.2	1.85	0.2	0	Rudder_Yx
Rudder_Y0.3	1.85	0.3	0	Rudder_Yx
Rudder_Y0.09	1.85	0.09	0	Rudder_Yx
Rudder_Y0.11	1.85	0.11	0	Rudder_Yx
Rudder_Y0.15	1.85	0.15	0	Rudder_Yx
Rudder_Y0.25	1.85	0.25	0	Rudder_Yx

Locations of the virtual hydrophones that can be seen in Table 4.1 are rotated from the [1, 0, 0] coordinate as the underwater glider model for logical comparison for 10° and -10° cases. Hydrophones that are elongate to the back of the vehicle, located in a straight line from the point of interest to improve the accuracy of the compared data with the 0° angle of attack case. Exact locations of the hydrophones for the 0° angle of attack case also transferred to other two cases in case of need of the data from these hydrophones.

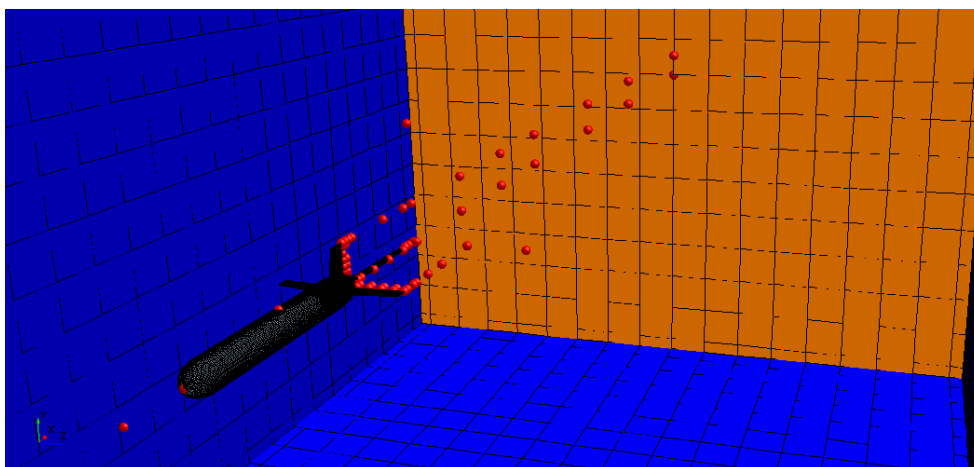


**Figure 4.11 :** Visualization of the first group virtual hydrophones for 0° angle of attack.

After the analysis of the values that are collected with the virtual hydrophones, hydrophones that are located outside of the refinement zones create abnormalities because of the decreasing resolution of mesh outside of the refinement zones. Therefore, hydrophones that are located outside of the refinement zones are not taken into account.





## 5. RESULTS AND DISCUSSION

Underwater glider case is analyzed in 3 different scenarios. These scenarios differ with changing angle of attack of the vehicle as  $0^\circ$ ,  $-10^\circ$  and  $10^\circ$ . Rotation of the vehicle is carried out only in XY plane because vehicle is symmetrical in other planes. Rudder of the vehicle disrupt the symmetry. In addition to that underwater sawtooth motion pattern of glider is simulated with the rotation in XY plane.

FW-H analogy is used with Farassat 1A equation in all cases to calculate the noise in the located virtual hydrophones with URANS turbulence model with considering k-epsilon in conjugation with the enhanced wall treatment model.

Results are given from the virtual hydrophones that are located in the turbulence zone to compare the noise level including the turbulence parameter/fields and to facilitate the comparison of the different angle of attack cases. Over All Sound Pressure Level of the points with the location of the hydrophones for all angle of attack cases in XY plane can be seen in Figure 5.1, 5.2 and 5.3. These hydrophones are located at from the back of the antenna (Xx) and rudder (Rudder\_Xx) to the 6 meters in the coordinate system. In these figure OASPLs at the top and bottom of the graphic are both positive with different start line to show the location of the hydrophones.

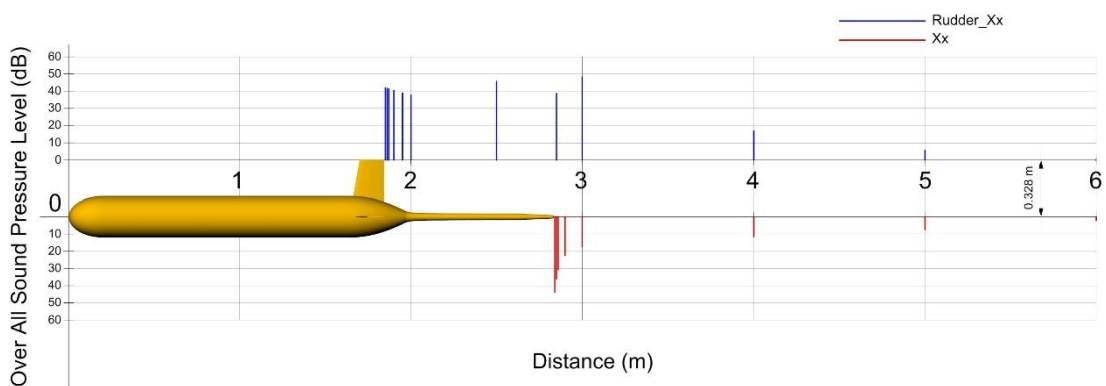


**Figure 5.1 :** OASPL values in XY plane for  $0^\circ$  angle of attack case (both directions show positive values).

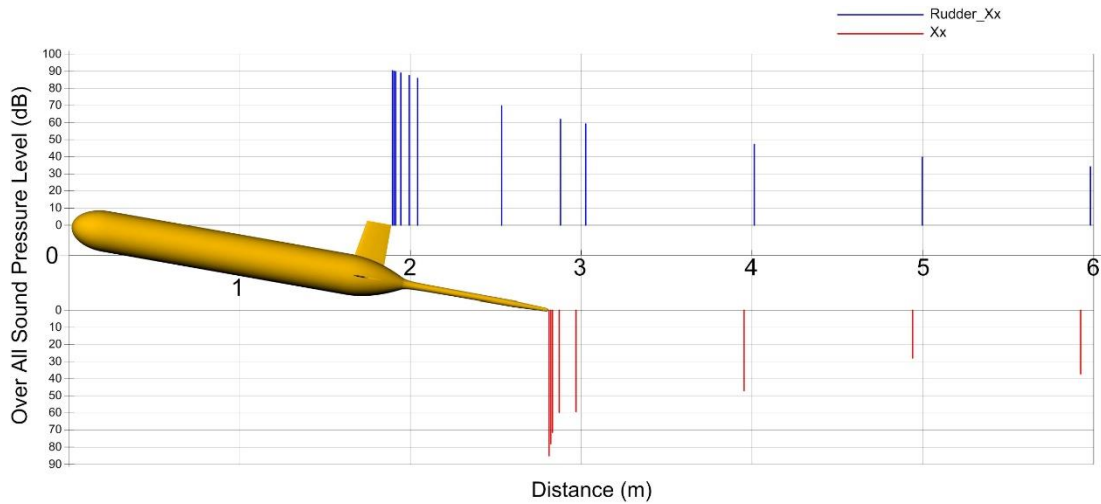


**Figure 5.2 :** OASPL values in XY plane for  $-10^\circ$  angle of attack case (both directions show positive values).



**Figure 5.3 :** OASPL values in XY plane for  $10^\circ$  angle of attack case (both directions show positive values).

Above figures shows that angle of attack is a crucial parameter for creation and propagation of the noise in fluid flow. Underwater gliders have to travel with an attack angle different than  $0^\circ$  to create lift force that results in horizontal movement. That's why  $10^\circ$  and  $-10^\circ$  attack angle cases shows the real life application situations although different underwater gliders can travel with different angle of attacks. Ascending ( $-10^\circ$  case) create slightly more noise in the rudder zone than descending ( $10^\circ$  case) as can be seen from Figure 5.2 and 5.3. The reason of this, vehicles body (hull) create distortion on the flow, enhance turbulence level on hull and flow field that increase the OASPL on that area. Additionally, Figure 5.2 and 5.3 shows that the orientation of the glider hull increase the noise that is created by flow at the back of the antenna. Explained effects of the flow field and flow parameters of all glider cases as velocity, turbulent kinetic energy (TKE) and pressure can be seen in Figure 5.4, 5.5 and 5.6.

These parameters affect the acoustic performance of the vehicle. That means improving glider hull and appendages designs will improve the acoustic signature and acoustic characteristics of the vehicle. Furthermore, deciding what will be the angle of attack of the vehicle throughout the expedition to decrease the acoustic signature for satisfying the mission needs, becomes easier.

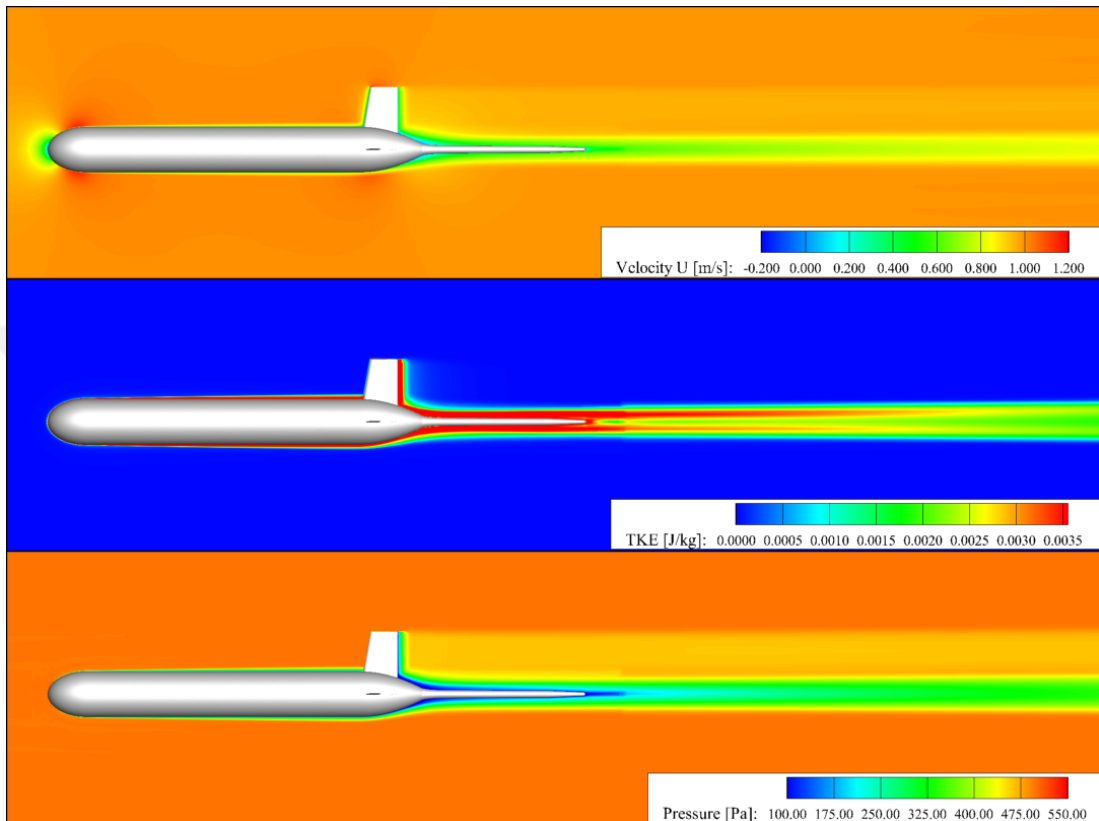


**Figure 5.4 :** Flow parameters (velocity, turbulent kinetic energy and pressure) and magnitudes of the 0° angle of attack case.

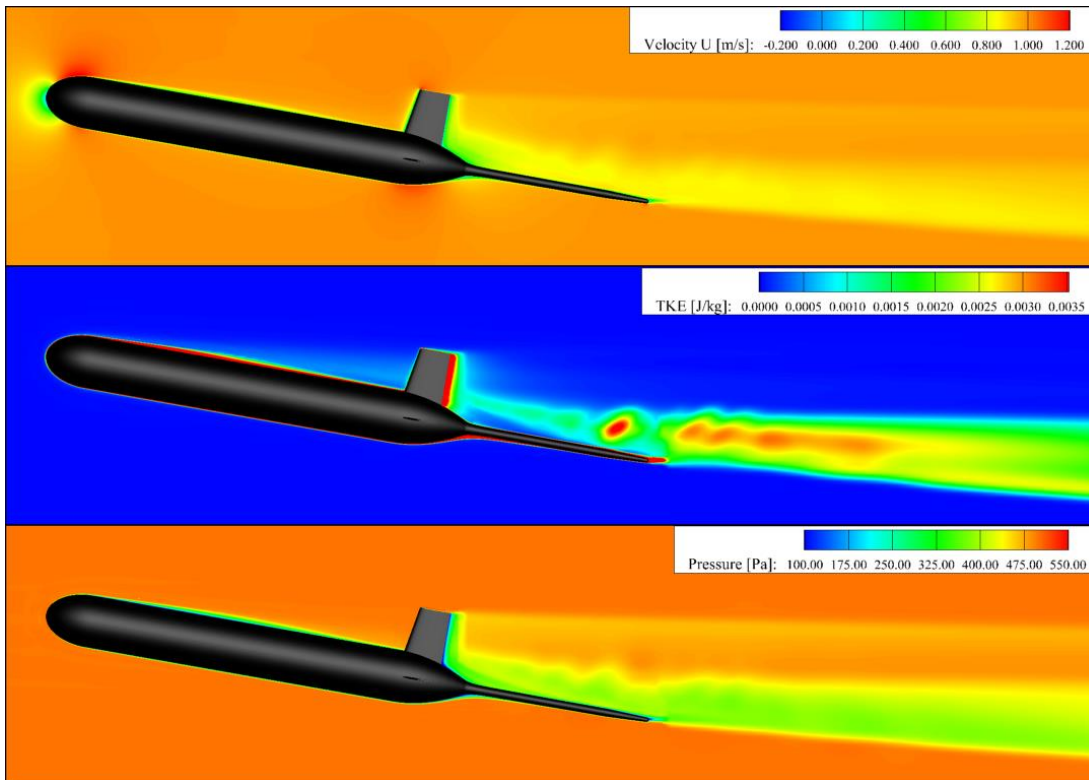


**Figure 5.5 :** Flow parameters (velocity, turbulent kinetic energy and pressure) and magnitudes of the  $-10^\circ$  angle of attack case.

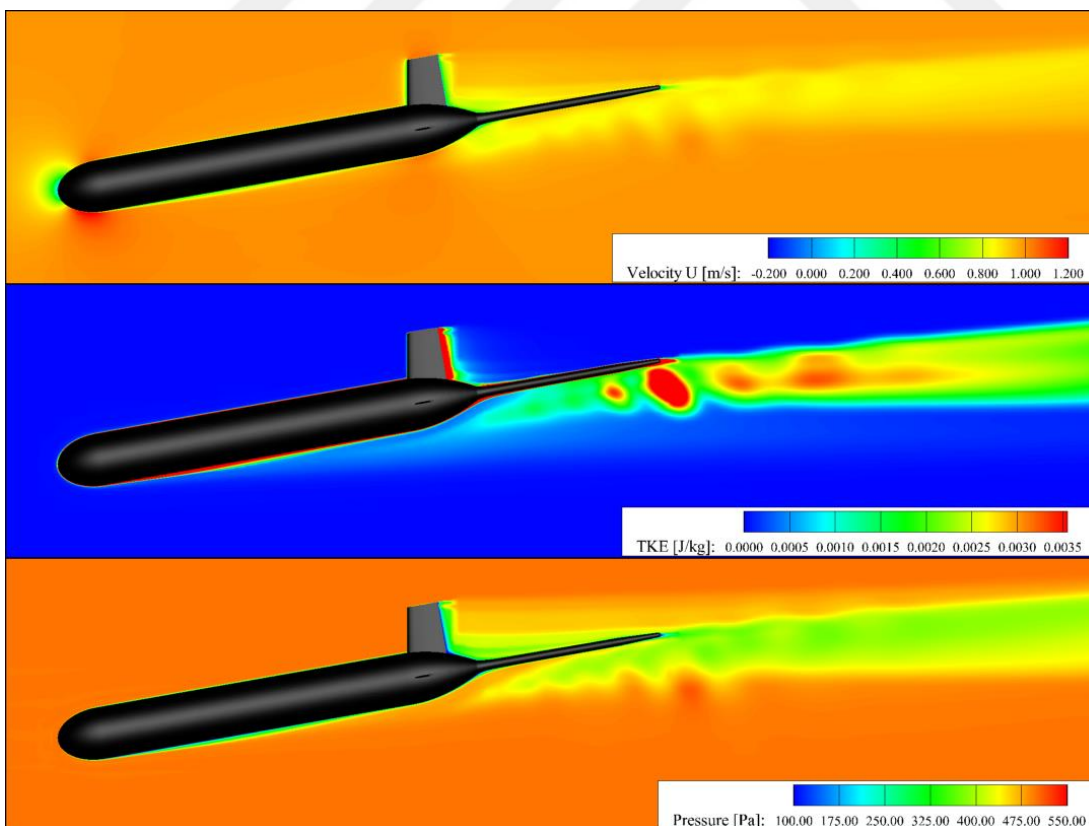


**Figure 5.6 :** Flow parameters (velocity, turbulent kinetic energy and pressure) and magnitudes of the  $10^\circ$  angle of attack case.

Surface pressure distribution also has significant effect on the flow noise because of the changing monopole and dipole terms. Changing the angle of attack affect the surface pressure distribution as can be seen in Figure 5.7. This comparison can be made using this parameter and Hull OASPL parameter in Figure 5.8, 5.9 and 5.10.

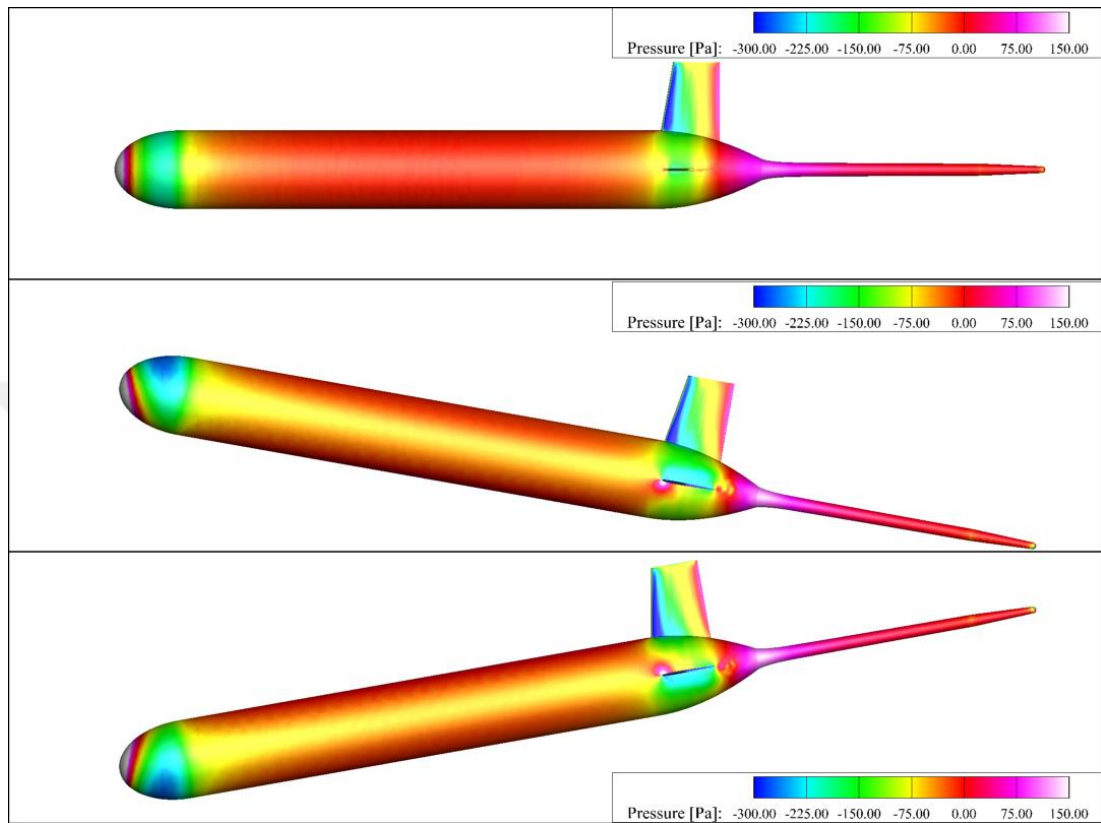


**Figure 5.7 :** Surface pressure distributions ( $0^\circ$ ,  $-10^\circ$ ,  $10^\circ$  respectively) and magnitudes of all cases.

Moreover, appendages of the glider are one of the significant factor for generation of the vorticity fields and high intensive turbulent motion. Noise waves are longitudinal vibrations; their propagation in a fluid flow is influenced by the presence of velocity gradients as well as the vorticity vectors. Therefore, acoustic analysis is also carried out at the back of the wings in XZ plane and OASPLs of these locations can be seen in Figure 5.8, 5.9 and 5.10 for 3 angle of attack cases.

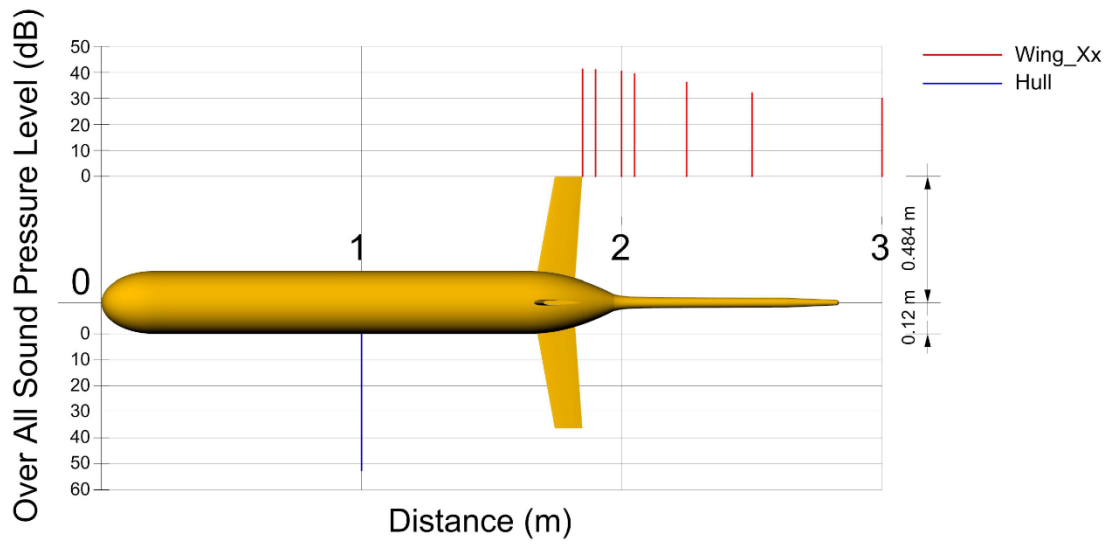


**Figure 5.8 :** OASPL values in XZ plane (top view) for 0° angle of attack case.

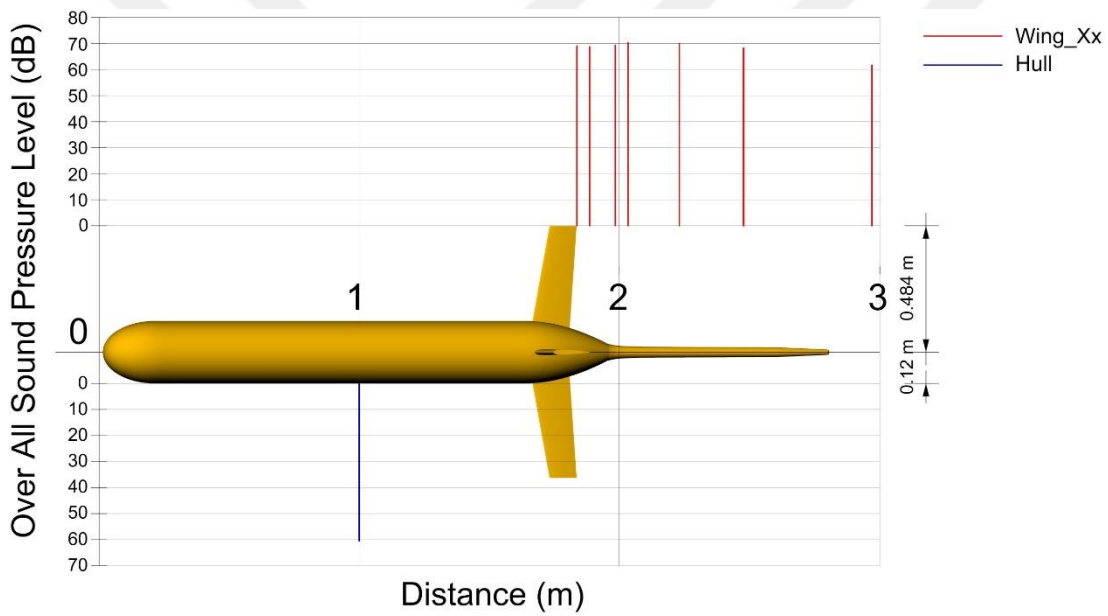


**Figure 5.9 :** OASPL values in XZ plane (top view) for -10° angle of attack case.

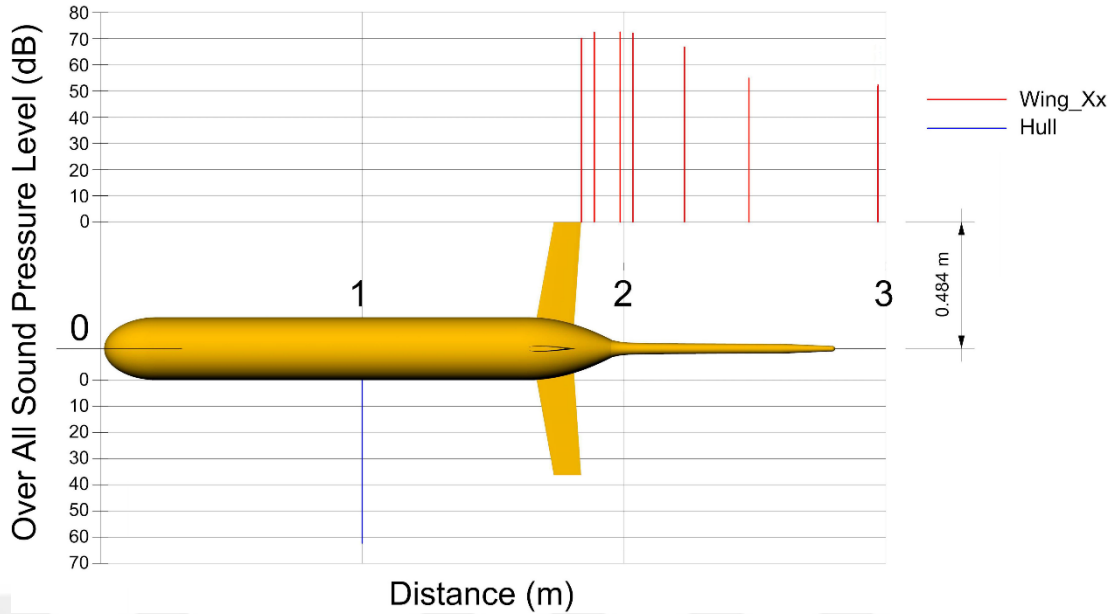


**Figure 5.10 :** OASPL values in XZ plane (top view) for  $10^\circ$  angle of attack case.

Underwater gliders need significant lift force compared to gravitational and buoyancy forces to increase the horizontal speed and range for decreasing the current effects on vehicle. To achieve this lift force, most of the gliders have large wing span. This situation increase the area and size of the appendages. Wings and rudder ends produce tip vortex and affect the acoustic performance of the vehicle as can be seen in above figures that shows the field that are at the end of the wing. Wings and rudder in this specific glider have symmetrical NACA airfoil form however different types of NACA form as NACA0006 and NACA0009 respectively. This alter the OASPL values when comparison is made between these zones in  $0^\circ$  angle of attack. Moreover comparing these cases with the validation case shows that form of the tip and general form of the appendages is substantial on acoustic performance.

As mentioned in section 2.2 FW-H analogy have 3 noise terms as loading, thickness and quadrupole. Loading (monopole) term is the dominant noise source in the marine cases that focus on flow noise as the 3 glider cases. Loading and thickness sound sources are formed over the surface. Therefore, sum of these two terms are called as Total Surface. Loading term is dominant in the near field for the glider cases and thickness terms converges to zero. However, loading terms diminishes with increasing distance from the vehicle. This explains the reduction of the noise at the far field. On the other hand quadrupole terms becomes effective in the far field as can be seen in Figure 5.11.

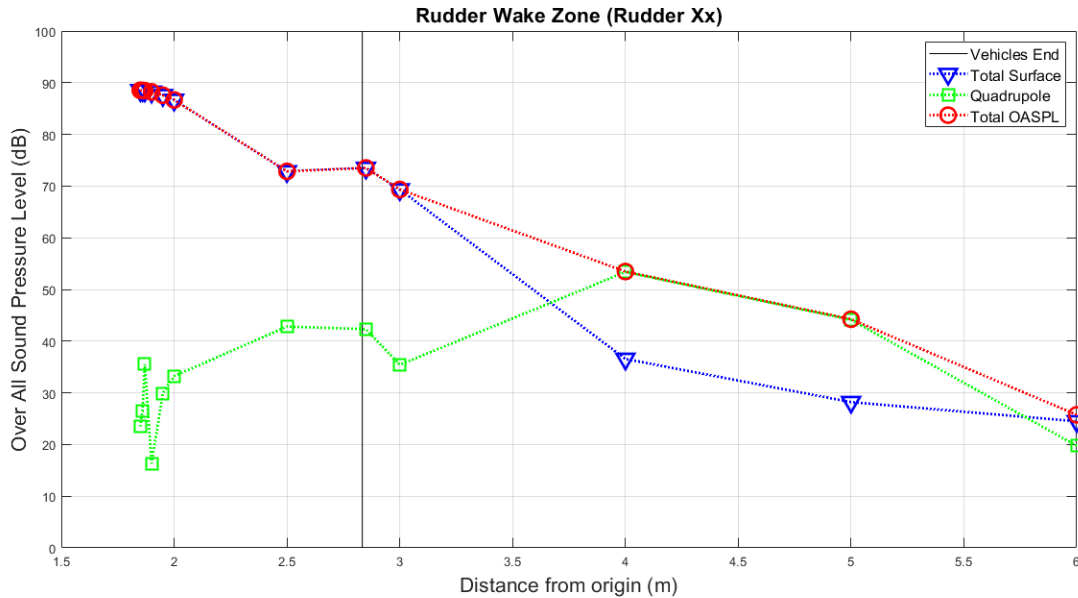


**Figure 5.11 :** Total Surface and Quadrupole terms of Rudder Zone at 10° angle of attack.

Calculation of the noise and relative change on specific areas can be related with the parameter of vorticity. Formerly, this is used in the acoustic cases to calculate the acoustic performance of the structure. This technique will not give the exact results. However it creates an opportunity for comparing the noise with the previous case. Vorticity is defined as the curl of the fluid and measure of local rotation of the fluid at a particular point. Fluid particle that have non zero vorticity means the particle is in rotational condition. As reverse, fluid particle that have zero vorticity means the particle is in irrotational state. Vorticity field around the hull and at the back of the vehicle for the 3 different angle of attack cases can be seen in Figure 5.12.

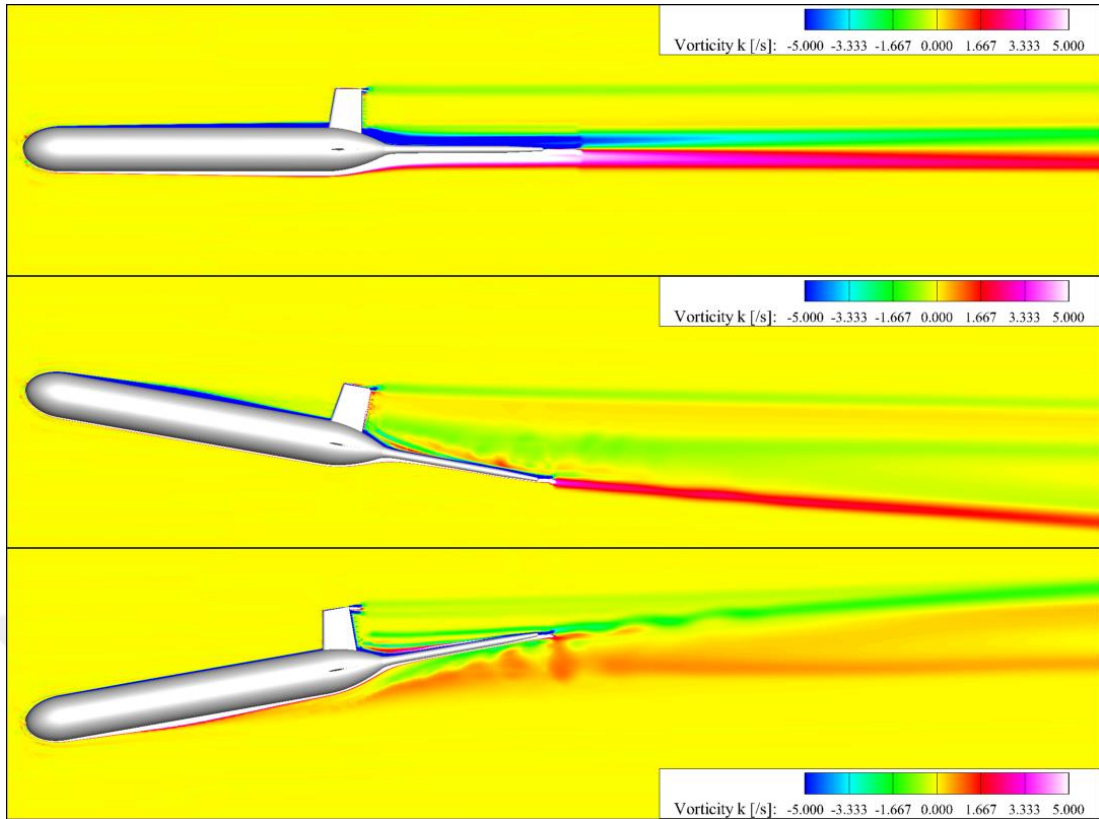


**Figure 5.12 :** Vorticity field for 3 different angle of attack cases.

Increasing vorticity magnitude increases the quadrupole term effect on the OASPL at the far field. This situation is analyzed at the back of the rudder. Moreover, increasing vorticity magnitude increases the total noise in the zones that are close to the vehicle. These conditions can be seen in Figure 5.13 that show the vorticity field at the back of the underwater glider in XY plane with the magnitudes. Points that are focused on also can be seen in that figure.

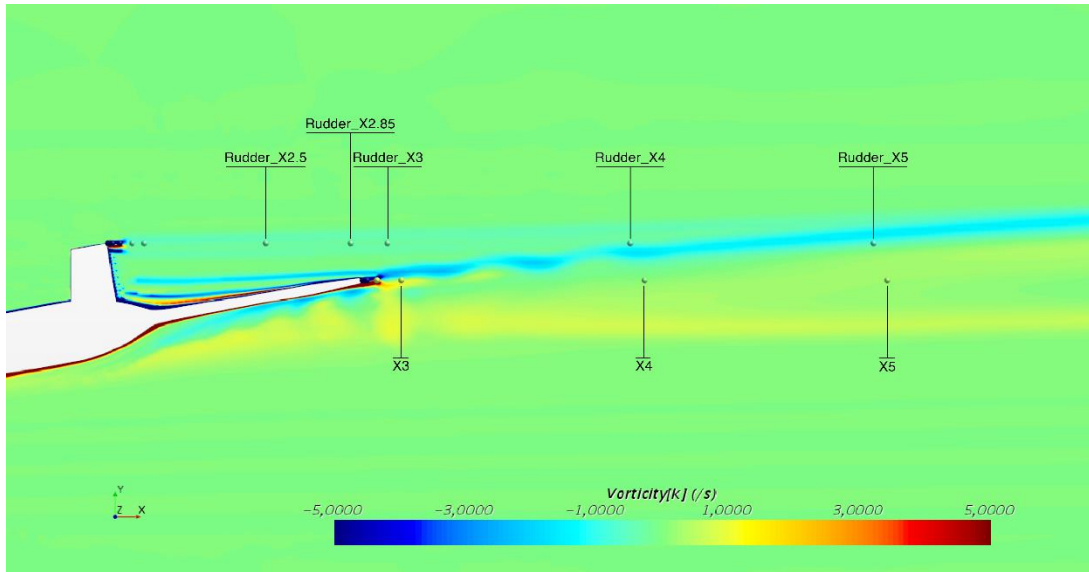


**Figure 5.13 :** Vorticity flow field at the back of the underwater glider in XY plane for 10° angle of attack.

As can be seen in Figure 5.13, high intensity vorticity flow field that comes from the back of the antenna is merged with the vorticity flow that comes from the back of the rudder. This creates more complex flow in that field where contain the hydrophones which are Rudder\_X4 and Rudder\_X5. This increases the quadrupole terms effect and increase the SPL that comes from quadrupole term. This increase in quadrupole term can be seen in Table 5.1. Table 5.1 shows that monopole terms effect decrease and quadrupole term becomes important with increasing distance from the vehicle. However as can be seen from the Table 5.1, Rudder\_X4 and Rudder\_X5’s quadrupole values increase rapidly when compared to total surface noise and becomes dominant in the zone where the high intensity vorticity flow field of the antenna and rudder merge.

**Table 5.1 :** Total surface and quadrupole values of the Rudder Zone hydrophones.

Receiver	Total Surface [dB]	Quadrupole [dB]	Total [dB]
Rudder_X6	24.4853	19.7465	25.74281
Rudder_X5	28.2003	44.1306	44.24006
Rudder_X4	36.5513	53.3772	53.46647
Rudder_X3	69.3375	35.4245	69.33926
Rudder_X2.85	73.509	42.3194	73.5123

## 6. CONCLUSION

Underwater gliders are unmanned, autonomous underwater vehicles that are mostly used for oceanographic surveys, oil and gas explorations and military activities. Underwater gliders main advantage is the endurance that can reach up to 12 months when compared with other UUVs. Long endurance is provided with the special propulsion mechanism. Underwater gliders use buoyancy engine to change their buoyancy to create vertical motion. Outside bladder is filled by pumping hydraulic oil to increase the total buoyancy of the vehicle to start ascending and oil is sucked into internal reservoir to decrease the total volume of the vehicle to start descending. This mechanism propel the vehicle. Pitch and yaw motions are created with the help of weight shifting mechanism and rudder. This propulsion mechanism also increase the stealthiness of the vehicle with no use of propellers. Pumps are used only to start the ascending or descending.

This movement mechanism of the vehicle decrease the structural noise to the minimum level with no turning or moving parts while gliding. However flow noise can still be a major factor for the reliability of the sensors that are located inside the vehicle and difficulty of the locating the vehicle from an outside source. Reducing the noise and noise signature of the vehicle also reduces the negative environmental effects, effect on the accuracy of the hydrophone data that is located in the underwater glider and increase the military capabilities of the vehicle.

In this thesis, acoustic characteristics of an underwater glider is analyzed. Simulations are carried out by using computational fluid dynamics methods considering 2 main case groups. First one is the validation case that is the comparison of the DARPA Suboff acoustic results with the experiment and literature. Second group is the cases of an underwater glider with varying angle of attack. Impact of the angle of attack on the noise production is examined. Moreover, hydrodynamic parameters like vorticity, velocity, turbulent kinetic energy and pressure influence on the acoustic results and on magnitude of the type of the sound source analyzed. FW-H acoustic analogy is used with the Farassat 1A formulation to calculate the total surface noise as well as the quadrupole noise. Turbulence is one of the major parameter for acoustic measurement

of the flow noise and modelled with the k-epsilon turbulence model from URANS turbulence model family with the enhanced wall treatment model. Underwater glider speed is selected 1 m/s which is generally the highest speed that the gliders can reach without propellers.

Results showed that even relatively slow vehicles like underwater gliders create significant flow noise. One of the main contributor of this flow noise is the appendages such as rudder and wings that create turbulence and tip vortex. In consequence of this, aeroacoustic noise increases as an impact of altering the physical parameters.

Underwater gliders need to travel with an angle of attack in order to create horizontal movement with created vertical movement by buoyancy engine. This propulsion mechanism increase the endurance of the vehicle and decrease the flow induced noise because of the minimum usage of machinery like propeller motors. However, angle of attack parameter increase the hydrodynamic noise by disturbing the flow and increasing turbulence. Optimization of this parameter for the mission has great importance when the acoustic performance of the vehicle is concerned. Results showed that, although in  $0^\circ$  angle of attack case maximum SPL is 70 dB, in  $-10^\circ$  angle of attack case maximum value increase to 102 dB, in  $10^\circ$  angle of attack case that value is 120 dB because of significant variation in the flow physics.

Monopole sound term is the dominant type of the sound in the marine cases and foremost contributor of the noise in the zones that are close to the vehicle. Increasing distance from the body reduces the effects of monopole terms and quadrupole term becomes dominant in some regions. Vorticity is one of the major factor for this transformation. Turbulent flow regions in far field increase the contribution of quadrupole term to the AOSPL values, especially regarding the angle of attack cases.

Underwater gliders can use hydrophones for detection of the underwater threats and capturing ambient noise. Marine mammals and their migration routes are analyzed with gathered data. In addition to the ambient noise, flow noise of the vehicle itself might disrupt this gathered data and makes it harder to separate the desired data from redundant data. Therefore, location of the hydrophone on the hull becomes a prominent subject during the design of the glider. Allocating the hydrophone from the peak noise zones of the vehicle can increase the accuracy of the data and makes post processing easier for the scientists.

Sound waves with low frequency have tendency to travel further than the high frequencies. Underwater glider cases revealed that the flow noise give peak SPL in the low frequencies (0-200 Hz). Therefore, created sound waves from the glider can be detected from a far distance with advanced hydrophones and sonars. Detection from a distance creates concern for military because of the need for stealth. Moreover, marine animals which use sound for locating the predators or prey and communication can be affected from the sound waves which have same frequency with radiated sound waves from themselves. This situation can cause behavioral change on the marine animals.

Essential purpose of this study is to specify the hydrodynamic and acoustic characteristics of underwater gliders. For this purpose, conditions of the vehicle are considered to reveal the hydrodynamic properties of an underwater glider as well as the noise signature. Furthermore, results show that the effects of the quadrupole noise terms need to be evaluated in marine applications. This thesis can be the first study on evaluation of relatively slow vehicles like the underwater gliders' aeroacoustics characteristics.

For the future work, same cases can be solved with different acoustic analogies for the comparison and validation of the FW-H analogy in the near and far field. Turbulence models of the URANS family decrease the computational time substantially with acceptable results. However, increasing the detail in the turbulent flow and creating cases which are close to the real life scenarios with LES turbulence model or advanced turbulence model will increase the accuracy of the data. The current work is mostly about capturing the overall acoustic trace of the glider. However, because the most important part of the noise is generated in the low frequency region, it is important to complete a longer duration simulation to be able to capture the low frequency sound waves. Moreover, analysis should run when the flow is fully developed. Results can be compared and differences need to be analyzed. These processes need considerable computational power and time.



## REFERENCES

- Abom, M.** (2010). *An Introduction to Flow Acoustics An introduction to Flow Acoustics* (4th ed.). KTH-The Royal Ins of Technology.
- Alobaid, F.** (2018). Computational fluid dynamics. In *Springer Tracts in Mechanical Engineering* (pp. 87–204). Springer International Publishing. [https://doi.org/10.1007/978-3-319-76234-0\\_3](https://doi.org/10.1007/978-3-319-76234-0_3)
- André, M., Morell, M., Mas, A., Solé, M., Schaar, M. van der, Houégnigan, L., ... Castell, J. V.** (2009). *Best Practices in Management, Assessment and Control of Underwater Noise Pollution. Laboratory of Applied Bioacoustics (LAB) Technical*. Barcelona.
- Autonomous Undersea Vehicle Applications Center.** (n.d.). The SeaExplorer underwater glider breaks World Record - AUVAC. Retrieved March 6, 2019, from <https://auvac.org/newsitems/view/2288>
- Bachmayer, R., Leonard, N. E., Graver, J., Fiorelli, E., Bhatta, P., & Paley, D.** (2004). Underwater gliders: recent developments and future applications. In *International Symposium on Underwater Technology*. Taipei: IEEE. <https://doi.org/10.1109/ut.2004.1405540>
- Bender, A., Steinberg, D. M., Friedman, A. L., & Williams, S. B.** (2008). Analysis of an Autonomous Underwater Glider. *Proceedings of the 2008 Australasian Conference on Robotics and Automation, ACRA 2008*.
- Bohn, D. A.** (1988). Environmental effects on the speed of sound. *Journal of the Audio Engineering Society*, 36(4).
- Bruneau, M.** (2006). *Fundamentals of Acoustics*. (S. F. D'Acoustique, Ed.), *Fundamentals of Acoustics* (1st ed.). London. <https://doi.org/10.1002/9780470612439>
- Chevalier, F., & Audoly, C.** (2013). Turbulent Flow-Induced Self Noise and Radiated Noise in Naval Systems—An Industry Point of View. In *Flinovia - Flow Induced Noise and Vibration Issues and Aspects*. Roma: Springer International Publishing. [https://doi.org/10.1007/978-3-319-09713-8\\_10](https://doi.org/10.1007/978-3-319-09713-8_10)
- Creasey, D. J.** (2003). *Fundamentals of marine acoustics. Coastal Engineering* (Vol. 2). [https://doi.org/10.1016/0378-3839\(78\)90017-0](https://doi.org/10.1016/0378-3839(78)90017-0)
- Dahl, P. H., Miller, J. H., Cato, D. H., & Andrew, R. K.** (2008). Underwater Ambient Noise. *Acoustics Today*, 3(1), 23–33. <https://doi.org/10.1121/1.2961145>
- Davis, R., Eriksen, C., & Jones, C.** (2002). Autonomous Buoyancy-Driven Underwater Gliders. In *Technology and Applications of Autonomous Underwater Vehicles* (pp. 37–58). <https://doi.org/10.1201/9780203522301.ch3>
- Diver's World.** (n.d.). ROV (Remotely Operated Vehicles). Retrieved March 6, 2019, from <https://www.antzoulis.gr/index.php/en/equipment/rov>

- Erbe, C.** (2013). International regulation of underwater noise. *Acoustics Australia*, 41(1), 12–19.
- Eriksen, C. C., Osse, T. J., Light, R. D., Wen, T., Lehman, T. W., Sabin, P. L., ... Chiodi, A. M.** (2001). Seaglider: A long-range autonomous underwater vehicle for oceanographic research. *IEEE Journal of Oceanic Engineering*, 26(4), 424–436. <https://doi.org/10.1109/48.972073>
- European Marine Strategy Framework Directive Good Environmental Status (MSFD-GES).** (2012). *Report of the Technical Subgroup on Underwater Noise and other forms of energy Final Report*. Retrieved from [www.milieu.be](http://www.milieu.be)
- Farassat, F.** (1975). *Theory of noise generation from moving bodies with an application to helicopter rotors*. NASA Langley Research Center. WASHINGTON, D. C.
- Farassat, F.** (2007). *Derivation of Formulations I and IA of Farassat*. NASA Langley Research Center. Hampton.
- Farassat, F., & Brentner, K. S.** (1987). The Uses and Abuses of the Acoustic Analogy in Helicopter Rotor Noise Prediction. *Journal of the American Helicopter Society*, 29–36. <https://doi.org/10.4050/jahs.33.29>
- Gamage, P. T.** (2017). *Modeling of flow generated sound in a constricted duct at low Mach number flow*. University of Central Florida. <https://doi.org/10.13140/RG.2.2.17805.03048>
- Griffiths, G., Jones, C., Ferguson, J., & Bose, N.** (2007). Undersea gliders. *Journal of Ocean Technology*.
- Groves, N. C., Huang, T. T., & Chang, M. S.** (1989). *Geometric characteristics of DARPA suboff models*. Dtrc/Shd-1298-01.
- Gustafsson, J.** (2016). *Mathematical Modelling and Solutions to Flow Acoustical Problems*. Chalmers University of Technology.
- Harland, E. J., Jones, S. a. S., & Clarke, T.** (2005). *SEA 6 Technical report: underwater ambient noise*. Qinetiq.
- Hart, J.** (2016). Comparison of Turbulence Modeling Approaches to the Simulation of a Dimpled Sphere. *Procedia Engineering*, 147, 68–73. <https://doi.org/10.1016/j.proeng.2016.06.191>
- IEEE Oceanic Engineering Society.** (n.d.). Going Deep to Go Far: How Dive Depth Impacts Seaglider Range | IEEE Earthzine. Retrieved March 6, 2019, from <https://earthzine.org/going-deep-to-go-far-how-dive-depth-impacts-seaglider-range/>
- Ikpekha, O. W.** (2017). *Underwater Acoustics Propagation Analysis and Modelling of Sound Emitting Devices*. DUBLIN CITY UNIVERSITY.
- Jacobsen, F., & Juhl, P. M.** (2013). *Fundamentals of General Linear Acoustics* (1st ed.). John Wiley & Sons, Ltd.
- Jenkins, S. A., & D'Spain, G.** (2016). Autonomous underwater gliders. In M. R. Dhanak, Florida Atlantic University, The Inst. for Ocean and Systems Engineering, & D. Beach (Eds.), *Springer Handbook of Ocean Engineering* (pp. 301–322). London: Springer International Publishing. [https://doi.org/10.1007/978-3-319-16649-0\\_12](https://doi.org/10.1007/978-3-319-16649-0_12)

- Kaltenbacher, M.** (2017). Theoretical Acoustics. *Journal of Computational Acoustics*, (March).
- Kellett, P.** (2014). *Integrated Prediction and Assessment of Underwater Noise for an LNG Carrier*. University of Strathclyde.
- Kongsberg Maritime.** (2014). *Seaglider*. Retrieved from [https://www.kongsberg.com/globalassets/maritime/km-products/documents/seaglider\\_product\\_specification.pdf](https://www.kongsberg.com/globalassets/maritime/km-products/documents/seaglider_product_specification.pdf)
- Kostaschuk, R., Best, J., Villard, P., Peakall, J., & Franklin, M.** (2005). Measuring flow velocity and sediment transport with an acoustic Doppler current profiler. *Geomorphology*, 68(1–2), 25–37. <https://doi.org/10.1016/j.geomorph.2004.07.012>
- Kuperman, W. A.** (2008). Acoustics, Deep Ocean. In *Encyclopedia of Ocean Sciences: Second Edition*. <https://doi.org/10.1016/B978-012374473-9.00312-X>
- L3 ASV.** (2016). Top 5 Things to Remember When Operating Unmanned Boats | L3 ASV | World Leading Marine Autonomy. Retrieved March 7, 2019, from <https://www.asvglobal.com/top-5-things-remember-operating-unmanned-boat/>
- Lighthill, M. J.** (1952). On sound generated aerodynamically I. General theory. *Proceedings of the Royal Society of London. Series A. Mathematical and Physical Sciences*, 211(1107), 564–587. <https://doi.org/10.1098/rspa.1952.0060>
- Liu, H.-L., & Huang, T. T.** (1998). *Summary of DARPA Suboff Experiment Program Data*. West Bethesda.
- Long, M. H., Rheuban, J. E., Berg, P., & Zieman, J. C.** (2012). A comparison and correction of light intensity loggers to photosynthetically active radiation sensors. *Limnology and Oceanography: Methods*, 10(6), 416–424. <https://doi.org/10.4319/lom.2012.10.416>
- Lu, Y., Zhang, H., & Pan, X.** (2008). Numerical Simulation of Flow Field and Flow Noise of Fully Attached Submarine. *Journal of Vibration and Shock*, 27.
- Lyrantzis, A. S.** (2003). Surface Integral Methods in Computational Aeroacoustics—From the (CFD) Near-Field to the (Acoustic) Far-Field. *International Journal of Aeroacoustics*, 95–128. <https://doi.org/10.1260/147547203322775498>
- Michael John Kingsford.** (n.d.). Marine ecosystem. Retrieved March 2, 2019, from <https://www.britannica.com/science/marine-ecosystem>
- National Research Council (US).** (2003). *Ocean Noise and Marine Mammals* (1st ed.). Washington, D.C.: National Academies Press. <https://doi.org/10.17226/10564>
- New Atlas.** (n.d.). Europe’s first ultra-deep-sea robotic glider to monitor deep sea pollution. Retrieved March 7, 2019, from <https://newatlas.com/bridges-ultra-deep-sea-robotic-glider/38336/>
- Popper, A. N., Hawkins, A. D., Fay, R. R., Mann, D. A., Bartol, S., Carlson, T. J., ... Tavalga, W. N.** (2014). *Sound Exposure Guidelines for Fishes and Sea Turtles. Springer Briefs in Oceanography*. London. <https://doi.org/10.1007/978-3-319-06659-2>

- Rudnick, D. L., Davis, R. E., Eriksen, C. C., Fratantoni, D. M., & Perry, M. J.** (2004). Underwater Gliders for Ocean Research. *Marine Technology Society Journal*, 38(2), 73–84. <https://doi.org/10.4031/002533204787522703>
- Russell, D. A., Titlow, J. P., & Bemmen, Y.-J.** (1999). Acoustic monopoles, dipoles, and quadrupoles: An experiment revisited. *American Journal of Physics*, 67(8), 660–664. <https://doi.org/10.1119/1.19349>
- Sodja, J., & Podgornik, R.** (2007). *Turbulence models in CFD*. University of Ljubljana. University of Ljubljana.
- Talley, L. D.** (2002). Salinity Patterns in the Ocean. In M. C. MacCracken & J. S. Perry (Eds.), *Encyclopedia of Global Environmental Change* (1st ed., pp. 629–640). John Wiley & Sons, Ltd.
- Testor, P., Meyers, G., Pattiaratchi, C., Bachmayer, R., Hayes, D., Pouliquen, S., ... Taillandier, V.** (2011). Gliders as a Component of Future Observing Systems. In *Proceedings of OceanObs'09: Sustained Ocean Observations and Information for Society* (pp. 961–978). San Diego: Scripps Institution of Oceanography. <https://doi.org/10.5270/oceanobs09.cwp.89>
- Unmanned Systems Technology.** (n.d.). General Dynamics Announces Availability of Bluefin SandShark AUV. Retrieved March 6, 2019, from <https://www.unmannedsystemstechnology.com/2017/01/general-dynamics-announces-availability-bluefin-sandshark-auv/>
- US Department of Commerce, N. O. and A. A.** (n.d.-a). What Is Ocean Exploration and Why Is It Important?: NOAA Office of Ocean Exploration and Research. Retrieved from <https://oceanexplorer.noaa.gov/backmatter/whatisexploration.html>
- US Department of Commerce, N. O. and A. A.** (n.d.-b). Why should we care about the ocean? Retrieved March 1, 2019, from <https://oceanservice.noaa.gov/facts/why-care-about-ocean.html>
- Williams, J. E. F., & Hawkings, D. L.** (1969). Sound Generation by Turbulence and Surfaces in Arbitrary Motion. *Philosophical Transactions of the Royal Society of London*, 264(1151), 321–342. <https://doi.org/10.1098/rsta.1969.0031>
- Woods Hole Oceanographic Institution.** (n.d.). WHOI Underwater Glider Operations. Retrieved March 6, 2019, from <http://gliders.whoi.edu/>
- Yao, H., Zhang, H., Liu, H., & Jiang, W.** (2017). Numerical study of flow-excited noise of a submarine with full appendages considering fluid structure interaction using the boundary element method. *Engineering Analysis with Boundary Elements*, 77, 1–9. <https://doi.org/10.1016/j.enganabound.2016.12.012>
- Yao, S., Guang, P., & Gao, H. Q.** (2013). LES-Based Numerical Simulation of Flow Noise for UUV with Full Appendages. *Advanced Materials Research*, 631, 879–884. <https://doi.org/10.4028/www.scientific.net/amr.631-632.879>
- Zhang, H., Fan, X., & Sun, H.** (2007). *Submarine Model Flow Noise Test Report, Technical report*.

## **CURRICULUM VITAE**

**Name Surname** : Turgay HIZARCI  
**Place and Date of Birth** : 26/04/1992 - İstanbul  
**E-Mail** : turgayhizarci@gmail.com

### **EDUCATION**

- **B.Sc.:** 2015 - Istanbul Technical University, Department of Shipbuilding and Ocean Engineering

### **PROFESSIONAL EXPERIENCE AND REWARDS**

- 2017 – Co-founder of Narval R&D
- 2019 - Research Assistant at Istanbul Technical University, Faculty of Naval Architecture and Ocean Engineering.

